40Ar–39 Ar dating, whole-rock and Sr-Nd isotope geochemistry of the Middle Eocene calc-alkaline volcanic rocks in the Bayburt area, Eastern Pontides (NE Turkey): Implications for magma evolution in an extension-related setting

Abdullah Kaygusuz, Cem Yücel, Emre Aydınçakır, Mehmet Ali Gücer, Gilles Ruffet

^{40}Ar–^{39}Ar dating, whole-rock and Sr-Nd isotope geochemistry of the Middle Eocene calc-alkaline volcanic rocks in the Bayburt area, Eastern Pontides (NE Turkey): Implications for magma evolution in an extension-related setting

Abdullah Kaygusuz [1] • Cem Yücel [2] • Emre Aydınçakır [1] • Mehmet Ali Gücer [1] • Gilles Ruffet [3, 4]

✉ Abdullah Kaygusuz
abdullah.kaygusuz@gmail.com

[1] Gümüşhane University, Department of Geological Engineering, TR-29000 Gümüşhane, Turkey

[2] Gümüşhane University, Department of Mining Engineering, TR-29000 Gümüşhane, Turkey

[3] CNRS (CNRS/INSU) UMR6118, Géosciences Rennes, Université de Rennes1, F-35042 Rennes Cedex, France

[4] Université de Rennes1, Géosciences Rennes, F-35042 Rennes Cedex, France

Abstract

Discussions continue about whether Middle Eocene magmatism in the Eastern Pontides is associated with collision or subduction. This paper presents new whole-rock geochemistry, Sr-Nd isotopic and ^{40}Ar-^{39}Ar age data for Middle Eocene volcanic rocks from the Bayburt area of the Eastern Pontides (NE Turkey) to investigate their sources and evolutionary history.

The new ^{40}Ar–^{39}Ar ages reveal that these volcanic rocks erupted between 44.6 ± 0.1 Ma and 43.5 ± 0.1 Ma, within the Lutetian (Middle Eocene). The studied volcanic rocks are composed of basalt, andesite, basaltic andesite and minor dacite lava and pyroclastic rocks. These rocks consist of plagioclase, amphibole, pyroxene, olivine, biotite, sanidine and minor quartz phenocrysts with Fe-Ti oxides. They have microlithic, hyalo-microlithic, porphyritic and rarely glomeroporphyritic textures. The volcanic rocks have low to high-K calc-alkaline affinities. They display enrichment in large-ion lithophile elements and depletion in high-field strength elements with high Th/Yb ratios, which indicate that the magmas forming the volcanic rocks were derived from lithospheric mantle sources enriched by mostly slab-derived fluids in the spinel stability field. $^{87}Sr/^{86}Sr_{(i)}$ values vary between 0.70485 and 0.70551 and $^{143}Nd/^{144}Nd_{(i)}$ values vary between 0.51255 and 0.51267. These data correspond to the mantle array on the isotope ratio diagram. The main solidification processes consist of fractional crystallization with minor assimilation. In light of the data obtained in this study together with data from previous studies, petrogenetic character of the Middle Eocene magmas from the southern parts of the Eastern Pontides may be explained by melting of an enriched lithospheric mantle source initially metasomatized by subduction fluids in a post-collisional extensional-related tectonic setting.

Keywords: $^{40}Ar/^{39}Ar$ geochronology • Post-collisional volcanism • Sr-Nd isotopes • NE Turkey • Eastern Pontides

Introduction

In orogenic belts, extensional tectonics usually develop during the post-orogenic phase after the completion of continent-continent collision. This occurs due to a combination of factors including the readjustment of the thickened lithosphere, lithospheric thinning by mantle convection, lithospheric collapse, slab break-off or detachment (Davies and von Blanckenburg 1995; Platt and England 1994; Ruppel 1995). The delamination of the mafic lower crust is usually associated with regions undergoing extension, showing thinning of the continental crust (Wang et al., 2008; Zhai et al., 2007).

The Eastern Pontides (NE Turkey, Fig. 1a), or the Eastern Sakarya Zone (ESZ), is a key area for understanding the geodynamic processes during the transition from pre- to post-orogenic stages and the temporal evolution of of compositions of syn- to post-collisional magmas. In the ESZ, the subduction and collision-related magmatic processes formed various types of igneous rocks. The subduction of the Neo-Tethyan Ocean beneath the Eurasian plate resulted in the development of the Pontide magmatic arc during the closure of the northern branch of the Neo-Tethyan, leading to the eventual collision of the Pontides and the Anatolide-Tauride block (ATB) in Late Palaeocene-Early Eocene (Yılmaz et al., 1997; Şengör and Yılmaz, 1981; Okay and Şahintürk 1997). The Middle Eocene volcanic activity in this region is related to a post-collisional geodynamic setting (Adamia et al., 1977; Kazmin et al., 1986; Şengör and Yılmaz, 1981; Robinson et al., 1995; Arslan et al., 1997; Okay and Şahintürk 1997; Altherr et al., 2008; Kaygusuz et al., 2011; Aydınçakır, 2014; Temizel et al., 2012).

The volcanism in the ESZ continued during Mesozoic and Cenozoic (Aydın et al., 2008; Eyuboğlu et al., 2011; Karslı et al., 2011; Dokuz et al., 2013; Arslan et al., 2013; Özdamar, 2016; Yücel et al., 2017). The Cenozoic volcanism is characterized by four magmatic cycles developed during the (1) Early Eocene, (2) Middle Eocene, (3) Late Eocene to Oligocene, and (4) Miocene to Pliocene (Topuz et al., 2005; Aydın et al., 2008; Karslı et

al., 2020; Temizel et al., 2012; Dokuz et al., 2013; Eyuboğlu et al., 2013a; Arslan et al., 2013; Aydınçakır and Şen, 2013; Aslan et al., 2014; Kaygusuz et al., 2011, 2019; Yücel et al., 2014). Volcanic rocks formed during the second cycle cover extensive areas within the ESZ, whereas rocks from the other three cycles are more localised (Fig. 1b). The third cycle associated with an extensional setting accompanied by the growth of extensional basins due to far-field extensional forces (Karslı et al., 2020), whereas the fourth cycle occurred in an extensional tectonic setting, combined with strike-slip movement at regional scale related to ongoing delamination (Yücel et al., 2017).

The second cycle magmatism in the ESZ developed during a compressional regime contemporaneous with the extensional regime associated with the opening of the Black Sea basin (Robinson et al., 1995; Okay et al., 1994; Ustaömer and Robertson, 1997; Görür and Tüysüz, 1997). However, the style and timing of Black Sea basin opening remain controversial (Shillington et al., 2008).

The detailed understanding of the evolution of the ESZ remains poorly constrained due to the scarcity of systematic geochronological, geochemical and isotopic data. In the southern zone of the ESZ, the geochemical, geochronological and isotopic properties of the Middle Eocene volcanic rocks (the second cycle) were studied around Torul-Gümüşhane (Kaygusuz et al., 2011), Gümüşhane (Aslan, 2010; Aslan et al., 2014) and Gümüşhane-Bayburt (Arslan et al., 2013). These rocks consist of mafic to felsic lava flows, dykes and associated pyroclastic deposits. They have clear subduction-related chemical signatures. The Bayburt area of the southern subzone within the ESZ is much less studied, with only general geology (Keskin et al., 1989), mineralogy and petrography (Kaygusuz et al., 2019), and whole-rock geochemistry (Eyuboğlu et al., 2017) described in the literature.

In this paper we present new ^{40}Ar–^{39}Ar dating, Sr–Nd isotope, and whole-rock geochemical data from the Middle Eocene volcanic rocks (the second cycle) in the Bayburt

area of the ESZ (Figs. 1b and c). The results will be used to constrain the genesis of calc-alkaline volcanism.

Geological background

Regional and local geology

The Pontides, which are one of the five main tectonic units forming the Anatolian Plate, are bounded by the Black Sea and the İstanbul zone to the north, and by the east-west trending İzmir-Ankara-Erzincan suture zone (IAES) to the south (Okay and Tüysüz, 1999) (Fig. 1a). The Pontide belt consists of three subunits: the eastern, central and western Pontides (Ketin and Canitez, 1972). The Eastern Pontides, also called the Eastern Sakarya Zone (ESZ), is part of the Sakarya Zone situated in the north of Turkey that extends from the Biga Peninsula to Lesser Caucasus. The ESZ is lithologically divided into two sub-zones; the northern subzone and the southern subzone (Özsayar et al., 1981). Most studies agree that the ESZ is a well-preserved continental magmatic arc. Magmatism in the ESZ covers a span from Carboniferous to the present.

The pre-Late Cretaceous rock units in the ESZ are represented by Early Carboniferous metamorphic rocks (Topuz et al., 2007), Middle to Late Carboniferous plutonic rocks (Kaygusuz et al., 2012, 2016; Dokuz., 2011; Topuz et al., 2010; Karslı et al., 2016), Late Carboniferous to Permian sedimentary rocks, Middle to Late Triassic plutonic rocks (Dokuz et al., 2010), Jurassic volcanic, volcaniclastic and plutonic rocks (Kandemir and Yılmaz, 2009; Saydam Eker et al., 2012; Dokuz et al., 2017; Aydınçakır et al., 2020) and Late Jurassic to Early Cretaceous carbonates (Pelin, 1977). All these rocks are conformably overlain by

Late Cretaceous volcanic rocks (Özdamar, 2016; Eyuboğlu, 2010; Aydın, 2014), and crosscut by plutonic rocks of late Cretaceous age (Şipahi et al., 2018; Karslı et al., 2010; Temizel et al., 2019; Kaygusuz et al., 2021). The Cenozoic rocks are represented by the first cycle adakitic rocks (Karslı et al., 2011; Topuz et al., 2005; Dokuz et al., 2013), the second cycle volcanic-subvolcanic (Aslan et al., 2014; Eyuboğlu et al., 2013b; Arslan et al., 2013; Aydınçakır, 2014; Yücel et al., 2017; Kaygusuz et al., 2011, 2019; Aydınçakır et al., 2022) and plutonic rocks (Karslı et al., 2007; Boztuğ et al., 2004; Özdamar et al., 2017; Eyuboğlu et al., 2017; Kaygusuz and Öztürk, 2015; Kaygusuz et al., 2018, 2020, 2021; Temizel et al., 2018, 2020; Vural and Kaygusuz, 2021), the third cycle volcanic rocks (Aydın et al., 2008; Arslan et al., 2013; Karslı et al., 2020) and the fourth cycle volcanic-subvolcanic and adakitic rocks (Temizel et al., 2012; Aydın et al., 2008; Dokuz et al., 2013; Yücel et al., 2017). Quaternary units comprise alluvium and terraces.

The study area is situated in the southern part of the ESZ (Fig. 1). The oldest rocks in the study area are represented by Late Cretaceous volcanic and volcaniclastic rocks, which are mainly composed of andesite, basalt and pyroclastic rocks (Fig. 2). The Early Eocene sedimentary rocks representing the first cycle lie conformably on this unit and consist mainly of nummulite-bearing limestones, sandstone, marl and sandy limestone. The Middle Eocene volcanic-volcaniclastic rocks, which represent the first cycle, conformably overlie these Early Eocene sedimentary units (Figs. 3a and b) and consist of basalt, andesite and minor dacite lavas and their pyroclastic equivalents, intercalated with siltstone, sandstone, marl and limestone. All these units were intruded by the second cycle plutonic rocks (43 to 45 Ma; Kaygusuz et al., 2020). Quaternary alluvium forms the youngest rocks in the study area.

Volcanic sequence

149 The Bayburt volcanic sequences extend in an east-west direction from Bayburt to Gümüşhane
150 areas in the southern part of the ESZ (Figs. 1b and 2). This sequence cover an area of 200 km^2
151 in the study area and contain limestones interbedded with sandstone and siltstone at the base
152 and pass upward into volcaniclastic rocks (tuff and agglomerate), lava flows and dykes.
153 Sedimentary and volcaniclastic rocks are widespread at the base, they become rarer upwards
154 and are replaced by lava flows.

155 The studied second cycle volcanic rocks consist of basalt, basaltic andesite, andesite
156 and minor dacite. Basalt and basaltic andesites are the dominant lithologies within the
157 sequence. Basalt contains subhedral to euhedral olivine, pyroxene and plagioclase
158 phenocrysts. Basaltic andesites have subhedral to euhedral plagioclase, pyroxene and
159 amphibole phenocrysts. Andesitic rocks are characterized by the presence of subhedral to
160 euhedral plagioclase, pyroxene and amphibole phenocrysts. Dacitic rocks comprise a minor
161 part of the sequence, and have large quartz phenocrystals. Dacites also contain subhedral to
162 euhedral plagioclase, amphibole and biotite phenocrysts.

163 The pyroclastic deposits are mainly composed of basaltic/andesitic breccias succeeded
164 by medium- to thick-bedded tuffs. Angular breccia gravels, 5 to 40 cm in diameter, are
165 cemented by a fine-grained, altered volcanic matrix. Basaltic, andesitic and minor dacitic tuffs
166 and tuffites have less volume than the other members in the sequence. Their cavities are filled
167 with secondary calcite, epidote and quartz minerals. In places where the unit is altered,
168 exfoliation structures are observed. The total thickness of the studied volcanic sequence in the
169 study area is more than 1300 m.

170 Basaltic lavas, which form the oldest lava in the succession, yield an $^{40}Ar/^{39}Ar$ age of
171 44.6 ± 0.1 Ma (this study, Table 1). They are overlain by basaltic andesitic lava flows with an
172 $^{40}Ar/^{39}Ar$ age of 44.0 ± 0.1 Ma (this study, Table 1). Andesitic lava flows crop out above

these rocks. Dacitic lavas, which are the youngest lava in the succession, conformably overlie these rocks and yield an $^{40}Ar/^{39}Ar$ age of 43.5 ± 0.1 Ma (this study, Table 1).

Material and methods

Rock samples were crushed in steel crushers and ground in an agate mill to a grain size of less than 200 mesh. Major elements were analyzed by inductively coupled plasma-emission spectrometry (ICP-ES) from pulps after 0.2 g samples of rock powder were fused with 1.5 g $LiBO_2$ and then dissolved in 100 ml 5% HNO_3. Trace and rare earth elements were determined by inductively coupled plasma-mass spectrometry (ICP-MS) from pulps after 0.2 g samples of rock powder were dissolved by four acid digestions. Sample solutions were aspirated into an ICP mass spectrometer (Perkin-Elmer Elan 6000) or an ICP emission spectrometer (Jarrel Ash Atomcomp Model 975) for element analyses. Loss on ignition (LOI) was determined according to the weight difference at 1000°C. Analytical precision, as calculated from replicate analyses, lies in the ranges of 0.01-0.04 wt% for the major elements and 0.01–8.0 ppm for trace elements including rare earth elements (REEs).

Three single groundmass fragments from the studied volcanic rocks were analysed by the continuous laser probe (CO_2 Synrad) stepwise heating ^{39}Ar-^{40}Ar technique. The samples were wrapped in Al foil to form small packets (11 mm × 11 mm) that were stacked up to form columns within which packets of fluence monitors were inserted every 10 samples. Irradiation was performed at the McMaster reactor (Hamilton, Canada) and used ^{5}C high flux location without Cd-shielding. It lasted 13.42 h ($J/h \approx 3.71 \times 10^{-4}\ h^{-1}$). The irradiation reference was sanidine TCRs (28.608 ± 0.033 Ma; according to Renne et al., 1998, 2010 and 2011). The sample arrangement in the irradiation allowed us to monitor the flux gradient with a precision

of ± 0.2 %. Heating steps were performed with a CO_2 laser probe. All experiments concerned single grains. The experimental procedure was described by Ruffet et al. (1991, 1995). The five argon isotopes and the background baselines were measured in 11 cycles, in peak-jumping mode. Blanks were performed routinely every first or third/fourth run and subtracted from subsequent sample gas fractions. All isotopic measurements are corrected for K, Ca and Cl isotopic interferences, mass discrimination and atmospheric argon contamination. Apparent age errors are plotted at the 2σ level and do not include the errors on the $^{40}Ar^*/^{39}Ar_K$ ratio and age of the monitor and decay constant. The errors on the $^{40}Ar^*/^{39}Ar_K$ ratio and age of the monitor and decay constant are included in the final calculation of the (pseudo-) plateau age error margins or for apparent ages individually cited. The analyses were performed on a Map215 mass spectrometer.

Sr and Nd isotopes from the studied volcanic rocks were conducted using thermal ionisation mass spectrometry (TIMS) on a Finnigan MAT-262 mass spectrometer. For Sr and Nd isotope analyses, approximately 50 mg of whole-rock powder was first dissolved in 52% HF for four days at 140 °C on a hot plate, then dried, dissolved in 6 N HCl, dried again and finally dissolved in 2.5 N HCl. Sr and Nd were separated using conventional ion exchange techniques. Isotopic compositions were measured on a double Re filament configuration. Total blanks were Sr-Nd-Sm < 0.05 ng; uncertainties were 2% for $^{87}Rb/^{86}Sr$ ratio and 0.2% for $^{147}Sm/^{144}Nd$ ratio. Sr and Nd isotope ratios were normalized to NBS987 ($^{87}Sr/^{86}Sr$ = 0.710179 ± 0.00001) and $JNd_{(i)}$ ($^{143}Nd/^{144}Nd$ = 0.511958 ± 0.000006; after Tanaka et al. (2000) standard. The values measured for these standards were 0.710246 ± 0.000010 and 0.512076 ± 0.000006, respectively.

Results

Petrography

Basalts have microlithic and microlithic–porphyritic textures (Fig. 3c). They consist of plagioclase, pyroxene, olivine phenocrysts and Fe-Ti oxides with a fine-grained groundmass. Basaltic andesites have generally microlithic to microlithic-porphyritic textures with phenocrysts of plagioclase, clinopyroxene and minor amphibole (Fig. 3d). The groundmass is composed of plagioclase microlites, small pyroxene grains and minor interstitial glass. Andesites exhibit hypo-crystalline porphyritic and glomeroporphyritic textures with phenocrysts of plagioclase, clinopyroxene, amphibole and minor biotite (Figs. 3e and f). The groundmass has a hyalopilitic texture and contains microliths of the main mineral constituents along with volcanic glass. Dacites exhibit microgranular, glomeroporphyritic and porphyritic textures characterized by plagioclase, amphibole, quartz and biotite phenocrysts set in a groundmass including microlites of the same minerals, Fe–Ti oxide and glass.

Plagioclase is the most abundant phenocryst and groundmass phase, and is found in all rock types. They exhibit albite twinning, oscillatory zoning, and prismatic-cellular growth. Phenocrysts are common in basaltic andesites, andesites and dacites. Anorthite content range between An_{88-49} in basalts, An_{83-46} in basaltic andesites, An_{60-35} in andesites, and An_{54-31} in dacites (Kaygusuz et al., 2019). Pyroxene forms subhedral to euhedral crystals and is found in glomeroporphyritic aggregates together with Fe-Ti oxides and plagioclase. The pyroxene phenocrysts consist of both ortho and clinopyroxene. Clinopyroxene phenocrystals (up to 2 mm) are the most common mafic mineral in the basaltic andesites. Pyroxenes are augite and diopside (Wo_{48-38} En_{46-38} Fo_{23-9}, Kaygusuz et al., 2019). Diopside and augite are found in basalts and basaltic andesites and augite in andesites (Kaygusuz et al., 2019). Inclusions of opaque minerals and plagioclase occur in large pyroxene crystals (2.5 mm) showing poikilitic

texture. Some minerals are partially altered to calcite and uralite. Amphibole occurs as both euhedral and subhedral phenocrystals and microlites in groundmass. They are found in basaltic andesite, andesite and dacite. Phenocrystals (2-2.5 mm) are common in basaltic andesites, andesites and dacites. Amphiboles are calcic magnesio-hornblende in composition (Kaygusuz et al., 2019). Some crystals show partial chloritization. Olivine is found as euhedral to subhedral crystals in basalt and basaltic andesite. Biotite, which is anhedral–subhedral, occurs in dacitic rocks and is rimmed by Fe–Ti oxide. Quartz is found in dacitic rocks, and embayed quartz crystals are common. Fe–Ti oxides occur mainly together with mafic minerals and are disseminated in the groundmass. They are magnetite–titanomagnetite in composition (Kaygusuz et al., 2019). Kaygusuz et al. (2019) indicated that the clinopyroxene pressure values of basalt, basaltic andesite and andesite range from 0.53 to 4.66 kbar and temperature values change from 1121 to 1182 °C. The clinopyroxene-liquid thermobarometer of Putirka (2008) and the only clinopyroxene core compositions were used to calculate the crystallisation temperature and pressure. Amphibole pressures and temperatures give values of 1.86 to 2.54 kbar and 788 to 872 °C for the andesitic and dacitic rocks (Kaygusuz et al., 2019). Al-in hornblende pressure calculations were made according to Johnson and Rutherford (1989) and amphibole-plagioclase temperature calculations according to Blundy and Holland (1990). Considering the thermobarometric calculations mentioned above, it is concluded that the calc-alkaline magma forming the Bayburt volcanic rocks equilibrated at shallow crustal depth.

^{40}Ar / ^{39}Ar geochronology

To determine the age of volcanic rocks, we separated groundmass fractions from one basalt, one basaltic andesite and dacite. The results are presented in Table 1, Table S1 and Fig 4. The

$^{40}Ar/^{39}Ar$ dating of the groundmass of basalt M-36 was performed in 14 heating steps and the age spectrum was defined by steps 9-14 with a plateau age 44.6 ± 0.1 Ma with 81.8% of the released ^{39}Ar (Fig. 4a, Table S1 in the electronic supplementary material, ESM). The isochron age for this sample is 44.5 ± 0.4 Ma with mean square of weighted deviates (MSWD)=1.76 (Fig. 4b, Table S1). $^{40}Ar/^{39}Ar$ dating of groundmass of basaltic andesite K-2 was performed in 14 heating steps. Steps 4-14 produced a plateau age of 44.0 ± 0.1 Ma with 92.8% of the released ^{39}Ar (Fig. 4c, Table S1). The isochron age of this sample is 43.9 ± 0.2 Ma with MSWD = 0.57 (Fig. 4d). $^{40}Ar/^{39}Ar$ dating of groundmass of dacite K-22 was performed in 15 steps (Table S1). The results suggest that the sample was affected by minor alteration or post-crystallization heating. However, steps 6-13 yielded a plateau age of 43.5 ± 0.1 Ma (Figs. 4e and f, Table S1). Obtained $^{40}Ar/^{39}Ar$ ages vary between 44.6 ± 0.1 and 43.5 ± 0.1 Ma, indicating that the studied volcanic rocks erupted in the Middle Eocene (Lutetian).

Geochemistry

Field and petrographic observations indicate that the studied volcanic samples in the Bayburt area suffered from minor alteration and partial chloritization and argillization. Most samples have loss on ignition (LOI) values <2.9 wt%, except for samples Y7 and Y35 that have LOI values of 3.5 and 3.1 wt%, respectively (Table 2).

Whole-rock compositions of the samples from the Bayburt volcanic rocks are given in Table 2. These volcanic rocks have a large range of SiO_2 contents (48 to 68 wt%) and Mg numbers [Mg# = 100×MgO/(MgO+Fe_2O_{3T})] (41 to 57; Table 2). The MgO and $Fe_2O_3^T$ contents range from 1.2% to 5.6% and from 3.5% to 10.6%, respectively (Table 2).

The samples plot in the sub-alkaline field on the TAS diagram (Fig. 5a). The samples show calc-alkaline affinity on the Th versus Co diagram (Fig. 5b). Most samples are located

298 in the calc-alkaline field in the AFM diagram, but a few samples plotted on the tholeiitic and
299 calc-alkaline division line (Fig. 5c). Andesitic rocks have medium-K composition, whereas
300 basaltic andesitic and andesitic rocks have high-K composition. Basalts have low to medium-
301 K composition (Fig. 5d).

302 Contents of CaO, Al_2O_3, Fe_2O_3, MgO, P_2O_5 and TiO_2 correlate negatively with SiO_2
303 (Fig. 6), whereas K_2O shows a positive correlation and Na_2O shows a weak positive
304 correlation. Positive correlations are seen for Ba, Th, Nb, Rb, Zr, Pb and La versus SiO_2, and
305 weak negative correlations are seen for Sr, Ni and Y (Fig. 6). Basaltic rocks have higher
306 MgO, CaO, $Fe_2O_3^T$, Al_2O_3, TiO_2 and Ni, whereas dacitic rocks have higher K_2O, Ba, Zr, Rb
307 and Nb contents than basaltic andesitic and andesitic rocks (Fig. 6).

308 On primitive mantle-normalized diagrams all samples exhibit significant enrichment
309 in large ion lithophile elements (LILEs) (K, Th, Rb) relative to high field strength elements
310 (HFSEs) and also negative Nb, Ti and Ta anomalies relative rare earth element (REE) of
311 similar incompatibility (Figs. 7a-d). All samples have similar LREE enriched patterns
312 revealed by enrichment in light rare earth elements (LREE) and nearly flat heavy rare earth
313 elements (HREE) (La_n/Sm_n=1.85 to 5.62, Gd_N/Lu_N= 1.14 to 2.16, Table 2, Figs. 7e-h).
314 Dacites are characterised by negative Eu (Eu_n/Eu^*) anomalies.
315

316 ## Sr-Nd isotope geochemistry

317

318 The studied samples have more radiogenic $^{87}Sr/^{86}Sr$ and less radiogenic $^{143}Nd/^{144}Nd$ isotopic
319 ratios than the bulk silica earth (BSE; Fig. 8a). The Bayburt volcanic rocks display relatively
320 homogeneous Sr-Nd isotopic compositions (Table 3; Fig. 8a). The values for $^{87}Sr/^{86}Sr_{(i)}$ range
321 from 0.70485 to 0.70551 and the values for $^{143}Nd/^{144}Nd_{(i)}$ range from 0.51255 to 0.51267
322 ($\varepsilon Nd = -0.71$ to $+1.76$), plotting within the mantle array (Fig. 8a; Table 3). Basalts and

basaltic andesites have lower $^{87}Sr/^{86}Sr_{(i)}$ values than andesites and dacites. A single-stage depleted mantle Nd model ages of the studied Bayburt samples are in the range of 0.71-1.01 Ga (Table 3).

The Bayburt volcanic rocks partly overlap with the other second cycle volcanic rocks from the ESZ (Kaygusuz et al., 2011; Aydınçakır and Şen, 2013; Arslan et al., 2013; Yücel et al., 2017; Aslan et al., 2014) and the second cycle plutonic rocks (Karslı et al., 2007; Eyuboğlu et al., 2017; Kaygusuz and Öztürk, 2015; Kaygusuz et al., 2020). However, they have higher Sr isotopic ratios than the first cycle volcanic rocks (Aydınçakır, 2014; Temizel et al., 2012, 2016), Early Eocene Kop adakitic rocks (Eyuboğlu et al., 2013a), the third cycle adakitic rocks (Karslı et al., 2020), the fourth cycle adakitic rocks (Eyuboğlu et al., 2012; Dokuz et al., 2013; Karslı et al., 2019) and the fourth cycle volcanic rocks (Temizel et al., 2012; Aydın et al., 2008; Yücel et al., 2017; Aslan et al. 2014). They have lower Sr isotopic ratios than the other first cycle adakitic rocks (Eyuboğlu et al., 2011, 2018; Karslı et al., 2010) (Fig. 8b).

Discussion

Age constraints

In previous studies, the age of the studied Bayburt volcanic rocks was estimated based on contact relationships, volcano-stratigraphic criteria and biostratigraphic data. Volcanic activity started in the Early Palaeocene and continued to Eocene time (Keskin et al., 1989). The new $^{40}Ar–^{39}Ar$ ages in this study place Bayburt volcanic rocks between 44.6 ± 0.1 Ma and 43.5 ± 0.1 Ma, within the Lutetian (the first cycle).

When compared with other Middle Eocene volcanic rocks in the ESZ, the new ^{40}Ar–^{39}Ar ages (44 to 43 Ma) of the studied Bayburt volcanic rocks are coeval with the Torul (Gümüşhane) volcanic rocks (43 Ma; Kaygusuz et al., 2011), Alucra-Bayburt volcanic rocks (44-43 Ma; Arslan et al., 2013) and Trabzon-Giresun volcanic rocks (44-43 Ma; Yücel et al., 2017). The Bayburt volcanic rocks are younger than the Gümüşhane tuffs (45 Ma; Aslan, 2010), Trabzon-Giresun basaltic-andesitic lava flows (45 Ma; Yücel et al., 2017) and Borçka volcanic rocks (46 Ma; Aydınçakır and Şen, 2013), but older than Trabzon-Giresun andesitic-trachytic dikes (42-41 Ma; Yücel et al., 2017) and Gümüşhane volcanic rocks (37 Ma; Aslan et al., 2014).

Fractional crystallization

The samples from the Bayburt volcanic rocks have low Mg#, MgO, Co, Ni and higher $^{87}Sr/^{86}Sr_{(i)}$ ratios demonstrating that the samples distinctively differ from primary magma composition and the magma has undergone significant fractional crystallization (FC; Tables 2 and 4).

Increasing K_2O, Zr, Rb, Ba, Th, Nb and Pb versus SiO_2 and the decreasing in CaO, $Fe_2O_3^T$, MgO, Al_2O_3, P_2O_5, TiO_2, Ni, Y and Sr content with increasing silica seen in basaltic to dacitic rocks indicate that they evolved via FC processes (Fig. 6). Decreasing TiO_2, P_2O_5 and Sr with increasing silica suggest fractionation of magnetite, apatite, and plagioclase, respectively (Fig. 6). Decreasing CaO suggests clinopyroxene fractionation. Increasing K_2O and Rb with increasing SiO_2 suggest that biotite and K-feldspar were not the early fractionation phases. Increasing silica with decreasing Sr and the negative Eu anomalies indicate plagioclase fractionation in the dacitic rocks (Figs. 6 and 7). The downward-concave

372 REE patterns of the rocks indicate clinopyroxene or hornblende fractionation (Thirlwall et al.,
373 1994).
374 The effectiveness of the FC process was tested by a Rb versus Y plot (Fig. 9a). Since
375 Rb has a positive correlation with the increase in SiO_2 (Fig. 6) content during fractionation,
376 Rb is used as the fractionation index. The Y content of the studied samples has a negative
377 correlation with the increasing Rb content (low-Y series), indicating plagioclase, clino-
378 pyroxene and hornblende fractionation (Fig. 9a).
379 On the MgO versus Sr diagram, all samples have negative correlation (Fig. 9b). This
380 correlation indicates fractionation of ferro-magnesian minerals occurred in basalt, basaltic
381 andesite and andesites, while feldspar fractionation occurred in dacitic rocks (Fig. 9b).
382

383 ## Assimilation - fractional crystallizations

384

385 The $^{87}Sr/^{86}Sr_{(i)}$ ratios correlate positively with SiO_2 and Th and negatively with. MgO (Figs.
386 10a, c and e). The $^{143}Nd/^{144}Nd_{(i)}$ ratios correlate negatively with SiO_2, and positively with
387 MgO and Sm/Nd (Figs. 10b, d and f). Such trends suggest that the magmas were affected by
388 assimilation - fractional crystallization processes. Assimilation of the crustal material was
389 accompanied fractional crystallization.
390 The roles of crustal assimilation and fractional crystallization processes were
391 evaluated using the equation described by DePaolo (1981). In our model, upper continental
392 crust values of Taylor and McLennan (1985) are used as crustal end-members, and the upper
393 mantle composition of Klein (2004) is used as parental magma composition. To estimate the
394 assimilation rate of the crust material by ascending magmas, different theoretical curves were
395 produced for the value of r = 0.2 (the ratio of the rate of assimilation to the rate of fractional
396 crystallisation) and the bulk distribution coefficients (D_{Sr}, D_{Nd}) (Fig. 11a, Table S2 in the

ESM). The studied Bayburt samples matched the r = 0.2 curves indicating that the parental magma was not significantly contaminated by continental crust (Fig. 11a). However, the above model can be considered as indicative only, as the modelled curve rely on appropriate values for the end-member compositions and Ds.

Mantle source

Among subduction-related magmas, those formed via addition of water-rich fluids to the mantle wedge generally have higher Ba/La ratios (Sheppard and Taylor, 1992; Elburg et al., 2002), Ba/Th (>170; Hawkesworth et al., 1997) and Pb/Ce (>0.1; Elburg et al., 2002), whereas magmas formed with the involvement of slab-derived melts and/or sediments are generally characterised by high Th/Ce ratios (>0.15; Hawkesworth et al., 1997). The mean values for Pb/Ce, Th/Ce and Ba/La ratios of the studied Bayburt volcanic rocks are 0.25, 0.09 and 20 (Table 2), respectively, indicating that water-rich fluids played an important role. This is also consistent with a range of Pb/Nd values at a constant $^{143}Nd/^{144}Nd_{(i)}$ (Fig. 11b) and with a wide range of. Ba/Th ratios of the least fractionated samples (SiO_2 <52 wt%) at similar La/Sm (Fig. 11c). A typical subduction-related incompatible-element pattern on mantle-normalised diagrams, characterised by prominent negative Nb and Ta anomalies (Fig 7), is also consistent with the important role of slab-derived fluids. Additionally, on the Ce/Pb versus Ce diagram (Fig. 11d), most of the samples correspond to the field of arc volcanics. The higher Th/Yb values at a given Ta/Yb compared to the mantle array (Fig. 11e; Pearce et al., 1990) is another evidence for addition of subduction related components. The trend displayed by the samples parallel to the mantle array can indicate either a range of variable enriched mantle source, or involvement of crustal assimilation.

Given that the least fractionated rocks (SiO_2 < 52 wt%) have low Mg# (54 to 44), MgO (5.55 to 3.14 wt%) and compatible trace element contents (Ni = 14.4 to 3.9 ppm and Co = 28.9 to 20.1 ppm; Table 2) are substantially evolved (cf. 500 to 600 ppm Cr, 250 to 300 ppm Ni, and 27 to 80 ppm Co in primary magmas; Wilkinson and Le Maitre, 1987; Perfit et al., 1980), no inferences on the mantle source composition of conditions of melting can be made.

Conclusions

Comprehensive whole-rock major, trace and rare earth elements, geochronological and Sr-Nd-Pb isotope data for the studied volcanic rocks from the southern part of the Eastern Pontides allow new insights into the petrogenetic evolution of the Middle Eocene magmas and enable us to reach the following conclusions. (i) The studied Bayburt volcanic rocks vary from basalt to dacite in composition, and define a calc-alkaline series showed enrichment of LILEs and LREEs, and depletion of HFSEs, suggesting similar sources and petrogenetic processes. (ii) ^{40}Ar-^{39}Ar ages of the rocks reveals that the studied volcanic rocks were emplaced in the Lutetian (44 to 43 Ma, Middle Eocene) and coincide with the time period of the post-collisional extensional regime in the Eastern Pontides. (iii) The Bayburt volcanic rocks have narrow initial $^{87}Sr/^{86}Sr$ ratios varying between 0.70485 and 0.70551 and initial $^{143}Nd/^{144}Nd$ values between 0.51255 and 0.51267 indicating enriched source composition. These data correspond to the mantle array on the isotope ratio diagram. (iv) The Bayburt volcanic rocks were mostly affected by fractional crystallization processes rather than the other magmatic processes, such as AFC, according to trace element chemistry, mineral chemistry and isotope data. (v) The studied volcanic rocks were generated from an enriched

lithospheric mantle source initially metasomatized by subduction fluids in a post-collisional extensional-related geodynamic setting.

Acknowledgements Thanks are due to Ferkan Sipahi, H. Enes Atay and Damla Selvi for their assistances in the fieldwork. The authors thanks David Vilbert for providing Sr-Nd isotopic analyses at the Géosciences Rennes, France. We thank an anonymous reviewer and journal editor Leonid V. Danyushevsky for their critical and constructive comments to improve our paper. This study has been funded by the Gümüşhane University Research Fund (grant 17.F5114.01.03).

References

Adamia SA, Lordkipanidze MB, Zakariadze GS (1977) Evolution of an active continental margin as exemplified by the Alpine history of the Caucasus. Tectonophysics 40:183–199

Altherr R, Topuz G, Siebel W, Şen C, Meyer HP, Satır M, Lahaye Y (2008) Geochemical and Sr–Nd–Pb isotopic characteristics of Paleocene plagioleucitites from the eastern Pontides (NE Turkey). Lithos 105:149–161

Arslan M, Temizel İ, Abdioğlu E, Kolaylı H, Yücel C, Boztuğ D, Şen C (2013) ^{40}Ar-^{39}Ar dating, whole-rock and Sr-Nd-Pb isotope geochemistry of post-collisional Eocene volcanic rocks in the southern part of the Eastern Pontides (NE Turkey): Implications for magma evolution in extension-induced origin. Contrib Mineral Petr 166/1:113–142

Arslan M, Tüysüz N, Korkmaz S, Kurt H (1997) Geochemistry and petrogenesis of the eastern Pontide volcanic rocks, Northeast Turkey. Chem Erde-Geochem 57:157–187

Aslan Z (2010) U-Pb zircon SHRIMP age, geochemical and petrographical characteristics of tuffs within calc-alkaline Eocene volcanic rocks around Gümüşhane (NE Turkey), Eastern Pontides. Neues Jb Miner Abh 187(3):329–346

Aslan Z, Arslan M, Temizel İ, Kaygusuz A (2014) K-Ar dating, whole-rock and Sr-Nd isotope geochemistry of calc-alkaline volcanic rocks around the Gümüşhane area: implications for post-collisional volcanism in the Eastern Pontides, Northeast Turkey. Miner Petrol 108:245–267

Aydın F (2014) Geochronology, geochemistry and petrogenesis of the Maçka subvolcanic intrusions: Implications for the Late Cretaceous magmatic and geodynamic evolution of the eastern part of the Sakarya Zone, NE Turkey. Inter Geol Rev 56(10):1246–1275

Aydın F, Karslı O, Chen B (2008) Petrogenesis of the Neogene alkaline volcanic rocks with implications for post collisional lithospheric thinning of the Eastern Pontides, NE Turkey. Lithos 104:249–266

Aydınçakır E (2014) The Petrogenesis of Early-Eocene non-adakitic volcanism in NE Turkey: Constraints on geodynamic implications. Lithos 208:361–377

Aydınçakır E, Gündüz R, Yücel C (2020) Emplacement conditions of magma(s) forming Jurassic plutonic rocks in Gümüşhane (Eastern Pontides, Turkey). Bull Min Res Exp 162:175–196

Aydınçakır E, Şen C (2013) Petrogenesis of the post-collisional volcanic rocks from the Borçka (Artvin) area: implications for the evolution of the Eocene magmatism in the Eastern Pontides (NE Turkey). Lithos 172–173:998–117

Aydınçakır E, Yücel C, Ruffet G, Gücer MA, Akaryalı E, Kaygusuz A (2022) Petrogenesis of post-collisional Middle Eocene volcanism in the Eastern Pontides (NE, Turkey): Insights from geochemistry, whole-rock Sr-Nd-Pb isotopes, zircon U-Pb and ^{40}Ar-^{39}Ar geochronology. Chem Erde-Geochem 82:125871

496 Blundy JD, Holland, TJB (1990) Calcic amphibole equilibria and a new amphibole-
497 plagioclase geothermometer. Contrib Mineral Petrol 104:208–224
498 Boztuğ D, Jonckheere R, Wagner GA, Yeğingil Z (2004) Slow Senonian and fast
499 Palaeocene–Early Eocene uplift of the granitoids in the Central eastern Pontides,
500 Turkey: apatite fission–track results. Tectonophysics 382:213–228
501 Davies JH, Von Blanckenburg F (1995) Slab breakoff: a model of lithospheric detachment
502 and its test in the magmatism and deformation of collisional orogens. Earth Planet Sc
503 Lett 129:85–102
504 DePaolo DJ (1981) Trace element and isotopic effects of combined wall-rock assimilation
505 and fractional crystallization. Earth Planet Sc Lett 53:189–202
506 Dokuz A (2011) A slab detachment and delamination model for the generation of
507 Carboniferous high-potassium I-type magmatism in the Eastern Pontides, NE Turkey:
508 Köse composite pluton. Gondwana Res 19:926–944
509 Dokuz A, Aydınçakır E, Kandemir R, Karslı O, Siebel W, Derman AS, Turan M (2017) Late
510 Jurassic magmatism and stratigraphy in the eastern Sakarya zone, Turkey: Evidence
511 for the slab breakoff of Paleotethyan oceanic lithosphere. J Geology 125:1–31
512 Dokuz A, Karslı O, Chen B, Uysal İ (2010) Sources and petrogenesis of Jurassic granitoids in
513 the Yusufeli area, northeastern Turkey: Implications for pre- and post-collisional
514 lithospheric thinning of the Eastern Pontides. Tectonophysics 480:259–279
515 Dokuz A, Uysal İ, Meisel W, Turan M, Duncan R, Akçay M (2013) Post-collisional adakitic
516 volcanism in the eastern part of the Sakarya zone, Turkey: Evidence for slab and
517 crustal melting. Contrib Mineral Petr 166:1443–1468
518 Elburg MA, Bergen MV, Hoogewerff J, Foden J, Vroon P, Zulkarnain I, Nasution A (2002)
519 Geochemical trends across an arc-continent collision zone: magma sources and

520 slabwedge transfer processes below the Pantar Strait volcanoes, Indonesia. Geochim
521 Cosmochim Ac 66:2771–2789
522 Eyuboğlu Y (2010). Late cretaceous high-K volcanism in the Eastern Pontide Orogenic Belt,
523 and its implications for the geodynamic evolution of NE Turkey. Int Geol Rev 52(2–
524 3):142–186
525 Eyuboğlu Y, Chung SL, Dudas FO, Santosh M, Akaryalı E (2011) Transition from
526 shoshonitic to adakitic magmatism in the Eastern Pontides, NE Turkey: implications
527 for slab window melting. Gondwana Res 19:413–429
528 Eyuboğlu Y, Dudas FO, Santosh M, Eroğlu-Gümrük T, Akbulut K, Yi K, Chatterje N (2018)
529 The final pulse of the Early Cenozoic adakitic activity in the Eastern Pontides
530 Orogenic Belt (NE Turkey): An integrated study on the nature of transition from
531 adakitic to non-adakitic magmatism in a slab window setting. J Asian Earth Sci
532 157:141–165
533 Eyuboğlu Y, Dudas FO, Santosh M, Yi K, Kwon S, Akaryali E (2013a) Petrogenesis and U-
534 Pb zircon chronology of adakitic porphyries within the Kop ultramafic massif (Eastern
535 Pontides Orogenic Belt, NE Turkey). Gondwana Res 24(2):742–766
536 Eyuboğlu Y, Dudas FO, Thorkelson D, Zhu DC, Liu Z, Chatterjee N, Yi K, Santosh M (2017)
537 Eocene granitoids of northern Turkey: Polybaric magmatism in an evolving arc–slab
538 window system. Gondwana Res 50:311–345
539 Eyuboğlu Y, Santosh M, Dudas FO, Akaryali E, Chung SL, Akdag K, Bektas O (2013b) The
540 nature of transition from adakitic to non-adakitic magmatism in a slab-window setting:
541 a synthesis from the eastern Pontides, NE Turkey. Geosci Front 4:353–375
542 Eyuboğlu Y, Santosh M, Yi K, Bektaş O, Kwon S (2012) Discovery of Miocene adakitic
543 dacite from the Eastern Pontides Belt and revised geodynamic model for the late
544 Cenozoic Evolution of eastern Mediterranean region. Lithos 146–147:218–232

545 Fitton JG, James D, Leeman WP (1991) Basic magmatism associated with Late Cenozoic
546 extension in the western United States: compositional variations in space and time. J
547 Geophysical Res 96:13693–13712
548 Görür N, Tüysüz O (1997) Petroleum geology of southern continental margin of the Black
549 Sea. In: A. Robinson (Ed.), Regional and Petroleum geology of the Black Sea and
550 Surrounding Region. AAPG Memoir 68:241-254
551 Güven İH (1993) 1:25000 Scale geology and compilation of the eastern Pontide. General
552 Directorate of Mineral Research and Exploration (MTA) of Turkey, Ankara
553 (unpublished).
554 Harms U, Cameron KL, Simon K, Bratz H (1997) Geochemistry and petrogenesis of
555 metabasites from the KTB ultradeep borehole, Germany Geol Rund 86:155–166
556 Hastie AR, Kerr AC, Pearce JA, Mitchell SF (2007) Classification of altered volcanic island
557 arc rocks using immobile trace elements: Development of the Th-Co discrimination
558 diagram. J Petrol 48:2341–2357
559 Hawkesworth C J, Turner SP, McDermott F, Peate DW, van Calsteren P (1997) U-Th
560 isotopes in arc magmas; implications for element transfer from the subducted crust.
561 Science 276:551–555
562 Hofmann AW (1988) Chemical differentiation of the Earth: The relationship between mantle,
563 continental crust, and oceanic crust. Earth Planet Sci Lett 90:297–314
564 Irvine TN, Baragar WRA (1971) A guide to the chemical classification of the common
565 volcanic rocks. Canadian J Earth Sci 8:523–548
566 Johnson MC, Rutherford MJ (1989) Experimental calibration of the aluminiun in hornblende
567 geobarometer with application to Long Valley Caldera (California) volcanic rocks.
568 Geology 17:837–841

569 Jung C, Jung S, Hoffer E, Berndt J (2006) Petrogenesis of Tertiary mafic alkaline magmas in
570 the Hocheifel, Germany. J Petrol 47:1637–1671
571 Kandemir R, Yılmaz C (2009) Lithostratigraphy, facies, and deposition environment of the
572 Lower Jurassic Ammonitico Rosso type sediments (ARTS) in the Gümüşhane area,
573 NE Turkey: Implications for the opening of the northern branch of the Neo-Tethys
574 Ocean. J Asian Earth Sci 34:586– 598
575 Karslı O, Caran Ş, Coban H, Şengün F, Tekkanat O, Andersen T (2020) Melting of the
576 juvenile lower crust in a far-field response to roll-back of the southern Neotethyan
577 oceanic lithosphere: the Oligocene adakitic dacites, NE Turkey. Lithos 105614:370–
578 371
579 Karslı O, Chen B, Aydın F, Şen C (2007) Geochemical and Sr-Nd-Pb isotopic compositions
580 of the Eocene Dölek and Sarıçiçek plutons, Eastern Turkey: Implications for magma
581 interaction in the genesis of high-K calc-alkaline granitoids in a post-collision
582 extensional setting. Lithos 98:67–96
583 Karslı O, Dokuz A, Kandemir R (2016) Subduction-related late Carboniferous to early
584 Permian magmatism in the eastern Pontides, the Camlik and Casurluk plutons:
585 Insights from geochemistry, whole-rock Sr-Nd and in situ zircon Lu-Hf isotopes, and
586 U-Pb geochronology. Lithos 266-267:98–114
587 Karslı O, Dokuz A, Kandemir R, Aydın F, Schmitt AK, Ersoy EY, Alyıldız C (2019)
588 Adakitic parental melt generation by partial fusion of the juvenile lower crust, Sakarya
589 Zone, NE Turkey: a far-field response to break-off of the southern Neotethyan oceanic
590 lithosphere. Lithos 338-339:58–72
591 Karslı O, Dokuz A, Uysal İ, Aydın F, Chen B, Kandemir R, Wijbrans J (2010) Relative
592 contributions of crust and mantle to generation of Campanian high-K calc-alkaline I-

593 type granitoids in a subduction setting, with special reference to the Harşit Pluton,
594 Eastern Turkey. Contrib Mineral Petr 160:467–487
595 Karslı O, Uysal I, Ketenci M, Dokuz A, Aydın F, Kandemir R, Wijbrans RJ (2011) Adakite-
596 like granitoid porphyries in Eastern Pontides, NE Turkey: potential parental melts and
597 geodynamic implications. Lithos 127:354–372
598 Kaygusuz A, Arslan M, Siebel W, Şen C (2011) Geochemical and Sr-Nd isotopic
599 characteristics of post-collisional calc-alkaline volcanic rocks in the eastern Pontides
600 (NE Turkey). Turk J Earth Sci 20:137–159
601 Kaygusuz A, Arslan M, Siebel W, Sipahi F, İlbeyli N (2012) Geochronological evidence and
602 tectonic significance of Carboniferous magmatism in the southwest Trabzon area,
603 eastern Pontides, Turkey. Int Geol Rev 54(15):1776–1800
604 Kaygusuz A, Arslan M, Sipahi F, Temizel İ (2016) U-Pb zircon chronology and petrogenesis
605 of Carboniferous plutons in the northern part of the Eastern Pontides, NE Turkey:
606 Constraints for Paleozoic magmatism and geodynamic evolution. Gondwana Res
607 39:327–346
608 Kaygusuz A, Arslan M, Temizel İ, Yücel C, Aydınçakır E (2021) U–Pb zircon chronology
609 and petrogenesis of the Late Cretaceous I-type granitoids in arc setting, Eastern
610 Pontides, NE Turkey. J African Earth Sci 174:104040
611 Kaygusuz A, Gücer MA, Yücel C, Aydınçakır E, Sipahi F (2019) Petrography and
612 crystallization conditions of Middle Eocene volcanic rocks in the Aydıntepe-Yazyurdu
613 (Bayburt) area, Eastern Pontides (NE Turkey). J Eng Res Appl Sci 8(2):1205–1215
614 Kaygusuz A, Öztürk M (2015) Geochronology, geochemistry, and petrogenesis of the Eocene
615 Bayburt intrusions, Eastern Pontides, NE Turkey: evidence for lithospheric mantle and
616 lower crustal sources in the high-K calc-alkaline magmatism. J Asian Earth Sci
617 108:97–116

618 Kaygusuz A, Yücel C, Arslan M, Sipahi F, Temizel İ, Çakmak G, Güloğlu ZS (2018)
619 Petrography, mineral chemistry and crystallization conditions of Cenozoic plutonic
620 rocks located to the north of Bayburt (Eastern Pontides, Turkey). Bull Min Res Exp
621 157:75–102
622 Kaygusuz A, Yücel C, Arslan M, Temizel İ, Yi K, Jeong YJ, Siebel W, Sipahi F (2020)
623 Eocene I-type magmatism in the Eastern Pontides, NE Turkey: Insights into magma
624 genesis and magma-tectonic evolution from whole-rock geochemistry, geochronology
625 and isotope systematics. Int Geol Rev 62(11):1406-1432
626 Kazmin VG, Sbortshikov IM, Ricou LE, Zonenshain LP, Boulin J, Knipper A (1986)
627 Volcanic belts as markers of the Mesozoic-Cenozoic evolution of Tethys,
628 Tectonophysics 123:123–152
629 Keskin İ, Korkmaz S, Gedik İ, Ateş M, Gök L, Küçümen Ö, Erkal T (1989) Bayburt
630 dolayının jeolojisi, MTA rap. No: 8995, 129 p, Ankara
631 Ketin İ, Canıtez N (1972) Yapısal jeoloji, İ.T.Ü Matbaası, Gümüşsüyü, 869, 520 p
632 Klein EM (2004) Geochemistry of the igneous oceanic crust. In: Treatise on geochemistry:
633 Holland HD, Turekian KK, (Ed.), Elsevier, Amsterdam, 3:433–463
634 Liew TC, Hofmann AW (1988) Precambrian crustal components, plutonic associations, plate
635 environment of the Hercynian Fold Belt of central Europe: indications from a Nd and
636 Sr isotopic study. Contrib Mineral Petrol 98:129–138
637 Middlemost EAK (1994) Naming materials in the magma/igneous rock system. Earth Sci Rev
638 37:215–224
639 Okay A, Şahintürk Ö (1997) Geology of the eastern Pontides. In: Robinson AG (ed.)
640 Regional and petroleum geology of the Black Sea and surrounding region. Am Assoc
641 Petr Geol B 68:291–311

642 Okay AI, Şengör AMC, Görür N (1994) Kinematic history of the opening of the Black Sea
643 and its effect on the surrounding regions: Geology 22:267–270
644 Okay AI, Tüysüz O (1999) Tethyan sutures of northern Turkey. In: Durand B, Jolivet L,
645 Horvath F, Seranne M (Eds.), Tethyan Sutures of Northern Turkey. Geol Soc Spec
646 Publ 156:475–515
647 Özdamar Ş (2016) Geochemistry and geochronology of late Mesozoic volcanic rocks in the
648 northern part of the Eastern Pontide Orogenic Belt (NE Turkey): implications for the
649 closure of the Neo-Tethys Ocean. Lithos 248–251:240–256
650 Özdamar Ş, Roden MF, Billor MZ (2017) Petrology of the shoshonitic Çambaşı Pluton in NE
651 Turkey and implications for the closure of the Neo-Tethys Ocean: insights from
652 geochemistry, geochronology and Sr–Nd isotopes. Lithos 284-285:477–492
653 Özsayar T, Pelin S, Gedikoğlu A (1981) Doğu Pontidler'de Kretase, KTÜ., Yerbilimleri
654 Dergisi 2:65–114
655 Pearce JA, Bender JF, De Long SE, Kidd WSF, Low PJ, Güner Y, Şaroğlu F, Yılmaz Y,
656 Moorbath S, Mitchell JJ (1990) Genesis of collision volcanism in eastern Anatolia
657 Turkey. J Volcanol Geoth Res 44:189–229
658 Pelin S (1977) Alucra (Giresun) GD yöresinin petrol olanakları bakımından jeolojik
659 incelemesi. KTÜ Yayın No: 87, Trabzon
660 Perfit MR, Gust DA, Bence AE, Arculus RJ, Taylor SR (1980) Chemical characteristics of
661 island-arc basalts: Implications for mantle sources, Chem Geol 30:227–256
662 Putirka KD (2008) Thermometers and barometers for volcanic systems. In: Putirka KD,
663 Tepley F (eds). Rev Mineral Geochem 69:61–120
664 Platt JP, England PC (1994) Convective removal of lithosphere beneath mountain belts:
665 Thermal and mechanical consequences. Am J Sci 294:307–336

Renne PR, Swisher CC, Deino AL, Karner DB, Owens TL, DePaolo DL (1998) Intercalibration of standards, absolute ages and uncertainties in $^{40}Ar/^{39}Ar$ dating. Chem Geol 145:117–152

Renne PR, Mundil R, Balco G, Min K, Ludwig KR (2010) Joint determination of ^{40}K decay constants and $^{40}Ar^*/^{40}K$ for the Fish Canyon sanidine standard, and improved accuracy for $^{40}Ar/^{39}Ar$ geochronology. Geochim Cosmochim Acta 74:5349–5367

Renne PR, Balco G, Ludwig KR, Mundil R, Min K (2011) Response to the comment by W.H. Schwarz et al. on "Joint determination of 40K decay constants and 40Ar∗/40K for the Fish Canyon sanidine standard, and improved accuracy for $^{40}Ar/^{39}Ar$ geochronology" by P.R. Renne et al., 2010. Geochim Cosmochim Acta 75:5097–5100

Robinson AG, Banks CJ, Rutherford MM, Hirst JPP (1995) Stratigraphic and structural development of the eastern Pontides, Turkey. J Geol Soc Lond 152:861–872

Ruffet G, Féraud G, Amouric M (1991) Comparison of $^{40}Ar/^{39}Ar$ conventional and laser dating of biotites from the North Trégor Batholith. Geochim Cosmochim Acta 55:1675–1688

Ruffet G, Féraud G, Ballèvre M, Kiénast JR (1995) Plateau ages and excess argon in phengites: an ^{40}Ar–^{39}Ar laser probe study of Alpine micas (Sesia Zone, Western Alps, northern Italy). Chem Geol 121:327–343

Ruppel C (1995) Extensional processes in continental lithosphere. J Geophysical Res 100,24:187–215

Saydam Eker Ç, Sipahi F, Kaygusuz A (2012) Trace and rare earth elements as indicators of provenance and depositional environments of Lias cherts in Gümüşhane, NE Turkey. Chem der Erde Geoc72:167–177

689 Schmidberger SS, Hegner E (1999) Geochemistry and isotope systematics of calc-alkaline
690 volcanic rocks from the Saar-Nahe basin (SW Germany)-implications for Late-
691 Variscan orogenic development. Contrib Mineral Petr 135:373–385
692 Sheppard S, Taylor WR (1992) Barium- and LREE-rich, olivine-mica-lamprophyres with
693 affinities to lamproites, Mt. Bundey, Northern Territory, Australia. In: Foley S. and
694 Peccerillo A. (Eds.), Potassic and ultrapotassic magmas and their origin; Sixth meeting
695 of the European Union of Geosciences. Lithos 28,3-6:303–325
696 Shillington DJ, White N, Minshull TA, Edwards GRH, Jones SN, Edwards RA, Scott CL
697 (2008) Cenozoic evolution of the eastern Black Sea: a test of depth-dependent
698 stretching models. Earth Planet Sc Lett 265:360–378
699 Sipahi F, Kaygusuz A, Saydam Eker Ç, Vural A, Akpınar İ (2018) Late Cretaceous arc
700 igneous activity: The Eğrikar Monzogranite example. Int Geol Rev 60/3:382-400
701 Sun SS, McDonough WF (1989) Chemical and isotope systematics of oceanic basalts;
702 implication for mantle compositions and processes. In: Saunders AD, Nory MJ (Eds.),
703 Magmatism in the Ocean Basins. Geol Soc London Spec Publ 42:313–345
704 Şengör AMC, Yılmaz Y (1981) Tethyan evolution of Turkey: a plate tectonic approach.
705 Tectonophysics 75:181–241
706 Tanaka T, Togashi S, Kamioka H, Amakawa H, Kagami H, Hamamoto T, Yuhara M,
707 Orihashi T, Yoneda S, Shimizu H, Kunimaru T, Takahashi K, Yanagi T, Nakano T,
708 Fujimaki H, Shinjo R, Asahara Y, Tanimizu M, Dragusanu C (2000) JNdi-1: a
709 neodymium isotopic reference in consistency with LaJolla neodymium. Chem Geol
710 168:279–281
711 Taylor SR, McLennan SM (1985) The Continental crust: Its composition and evolution.
712 Blackwell Publication, Oxford

713 Temizel İ, Abdioğlu Yazar E, Arslan M, Kaygusuz A, Aslan Z (2018) Mineral chemistry,
714 whole-rock geochemistry and petrology of Eocene I-type Shoshonitic plutons in the
715 Gölköy area (Ordu, NE Turkey). Bull Min Res Exp 157:121–152
716 Temizel İ, Arslan M, Ruffet G, Peucat JJ (2012) Petrochemistry, geochronology and Sr-Nd
717 isotopic systematics of the Tertiary collisional and post-collisional volcanic rocks from
718 the Ulubey (Ordu) area, eastern Pontide, NE Turkey: implications for extension-
719 related origin and mantle source characteristics. Lithos 128:126–147
720 Temizel İ, Arslan M, Yücel C, Abdioğlu Yazar E, Kaygusuz A, Aslan Z (2020) Eocene
721 tonalite–granodiorite from the Havza (Samsun) area, northern Turkey: Adakite-like
722 melts of lithospheric mantle and crust generated in a post-collisional setting. Int Geol
723 Rev 62(9):1131–1158
724 Temizel İ, Arslan M, Yücel C, Abdioğlu Yazar E, Ruffet G (2016) Geochronology and
725 geochemistry of Eocene-aged volcanic rocks around the Bafra (Samsun, N Turkey)
726 area: constraints for the interaction of lithospheric mantle and crustal melts. Lithos
727 258–259:92–114
728 Temizel İ, Arslan M. Yücel C. Abdioğlu Yazar E, Kaygusuz A, Aslan Z (2019) U-Pb
729 geochronology, bulk-rock geochemistry and petrology of Late Cretaceous syenitic
730 plutons in the Gölköy (Ordu) area (NE Turkey): Implications for magma generation in
731 a continental arc extension triggered by slab roll-back. J Asian Earth Sci 171:305–320
732 Thirlwall MF, Smith TE, Graham AM, Theodorou N, Hollings P, Davidson JP, Arculus RJ
733 (1994) High field strength element anomalies in arc lavas; source or process? J Petrol
734 35/3:819–838
735 Topuz G, Alther R, Schwarz WH, Siebel W, Satır M, Dokuz A (2005) Post-collisional
736 plutonism with adakite-like signatures: the Eocene Saraycık granodiorite (eastern
737 Pontides, Turkey). Contrib Mineral Petr 150:441–455

738 Topuz G, Altherr R, Schwarz WH, Dokuz A, Meyer HP (2007) Variscan amphibolite facies
739 metamorphic rocks from the Kurtoğlu metamorphic complex (Gümüşhane area,
740 eastern Pontides, Turkey). Int J Earth Sci 96:861–873
741 Topuz G, Altherr R. Siebel W, Schwarz WH, Zack T, Hasözbek A, Barth M, Satır M, Şen C
742 (2010) Carboniferous high-potassium I-type granitoid magmatism in the eastern
743 Pontides: the Gümüşhane pluton (NE Turkey). Lithos 116:92–110
744 Ustaömer T, Robertson AHF (1997) Tectonic-sedimentary evolution of the North-Tethyan
745 active margin in the Central Pontides of Northern Turkey. In: Robinson, A.G. (ed),
746 Regional and Petroleum Geology of the Black Sea Region. Am Assoc Petr Geol M
747 68:245–290
748 Vural A, Kaygusuz A (2021) Geochronology, petrogenesis and tectonic importance of Eocene
749 I-type magmatism in the Eastern Pontides, NE Turkey. Arab J Geocsi 14:467.
750 https://doi.org/10.1007/s12517-021-06884-z
751 Wang XL, Zhao G, Zhou JC, Liu Y, Hu J (2008) Geochronology and Hf isotopes of zircon
752 from volcanic rocks of the Shuangqiaoshan group, south China: Implications for the
753 Neoproterozoic tectonic evolution of the eastern Jiangnan orogen. Precambrian Res
754 14:355–367
755 Wilkinson JFG, Le Maitre RW (1987) Upper mantle amphiboles and micas and TiO_2, K_2O,
756 and P_2O_5 abundances and 100 Mg/(Mg + Fe^{2+}) ratios of common basalts and
757 andesites: Implications for modal mantle metasomatism and undepleted mantle
758 compositions. J Petrol 28:37–7
759 Yılmaz Y, Tüysüz O, Yiğitbaş E, Genç SC, Şengör AMC (1997) Geology and tectonics of the
760 Pontides. In: Robinson, A.G. (Eds.), Regional and petroleum geology of the Black Sea
761 and surrounding region. Am Assoc Petr Geol B 68:183–226

762 Yücel C, Arslan M, Temizel İ, Abdioğlu E (2014) Volcanic facies and mineral chemistry of
763 Tertiary volcanic rocks in the northern part of the Eastern Pontides, northeast Turkey:
764 implications for pre-eruptive crystallization conditions and magma chamber processes.
765 Miner Petrol 108:439–467
766 Yücel C, Arslan M, Temizel I, Yazar EA, Ruffet G (2017) Evolution of K-rich magmas
767 derived from a net veined lithospheric mantle in an ongoing extensional setting:
768 geochronology and geochemistry of Eocene and Miocene volcanic rocks from Eastern
769 Pontides (Turkey). Gondwana Res 45:65–86
770 Zhai MG, Fan QC, Zhang HF, Sui JL, Shao JA (2007) Lower crustal processes leading to
771 Mesozoic lithospheric thinning beneath eastern North China: underplating,
772 replacement and delamination. Lithos 96:36–54

773 **FIGURE CAPTIONS**

774

775 **Fig. 1 (a)** Tectonic map of Turkey and its surroundings (modified from Okay and Tüysüz,
776 1999), **(b)** Simplified geological map of the Eastern Pontides showing the distribution of
777 Eocene and Miocene volcanic rocks and Eocene plutonic rocks (modified from Arslan et al.,
778 2013; Güven, 1993; Temizel et al., 2016). NAFZ – North Anatolian Fault Zone

779

780 **Fig. 2** Geological map of the study area

781

782 **Fig. 3** Field view and cross-polarised transmitted-light photomicrographs of textural features
783 of the studied Bayburt volcanic rocks **(a)** Field view of the contact between Eocene
784 sedimentary and volcanic rocks, **(b)** field view of Eocene volcanic rocks, **(c)** microlithic
785 textures in basalts, and **(d-f)** microlithic-porphyritic and glomeroporphyritic textures in
786 basaltic andesites and andesites (Pl: plagioclase, Cpx: clinopyroxene, Amp: amphibole)

787

788 **Fig. 4** ^{40}Ar-^{39}Ar ages of the Bayburt volcanic rocks, **(a-b)** basalt (M-36), **(c-d)** basaltic
789 andesite (K-2) and **(e-f)** dacite (K-22)

790

791 **Fig. 5 (a)** Silica versus total alkalis diagram (after Middlemost, 1994), **(b)** Th versus Co
792 diagram (after Hastie et al., 2007), **(c)** AFM diagram of Irvine and Baragar (1971), and **(d)**
793 K_2O versus SiO_2 diagram for Bayburt volcanic rocks

794

795 **Fig. 6 (a-r)** SiO_2 versus major oxides, trace elements and rare earth elements variation plots
796 for Bayburt volcanic rocks

797

Fig. 7 (a-d) Primitive mantle-normalized (Sun and McDonough, 1989) trace element patterns, **(e-h)** chondrite-normalized (Taylor and McLennan, 1985) rare earth element patterns for Bayburt volcanic rocks

Fig. 8 (a-b) $^{143}Nd/^{144}Nd_{(i)}$ versus $(^{87}Sr/^{86}Sr)_{(i)}$ diagrams for Bayburt volcanic rocks

Fig. 9 (a) Y versus Rb, and **(b)** MgO versus Sr diagrams for Bayburt volcanic rocks

Fig. 10 (a-b) SiO_2 versus $^{87}Sr/^{86}Sr_{(i)}$ and $^{143}Nd/^{144}Nd_{(i)}$, **(c-d)** MgO (wt%) versus $^{87}Sr/^{86}Sr_{(i)}$ and $^{143}Nd/^{144}Nd_{(i)}$, **(e)** $^{87}Sr/^{86}Sr_{(i)}$ versus Th, and **(f)** $^{143}Nd/^{144}Nd_{(i)}$ versus Sm/Nd diagrams for Bayburt volcanic rocks

Fig. 11 (a) $(^{87}Sr/^{86}Sr)_{(i)}$ versus $(^{143}Nd/^{144}Nd)_{(i)}$ diagram showing two-component mixing model, **(b)** Pb/Nd versus $(^{143}Nd/^{144}Nd)_{(i)}$, **(c)** Ba/Th versus La/Sm, **(d)** Ce/Pb versus Ce (ppm), and **(e)** Th/Yb versus Ta/Yb (after Pearce et al., 1990) diagrams for Bayburt volcanic rocks. (d): Data fields after Taylor and McLennan (1985), Hofmann (1988), Harms et al. (1997), Schmidberger and Hegner (1999), Pearce et al. (1990), Fitton et al., (1991)

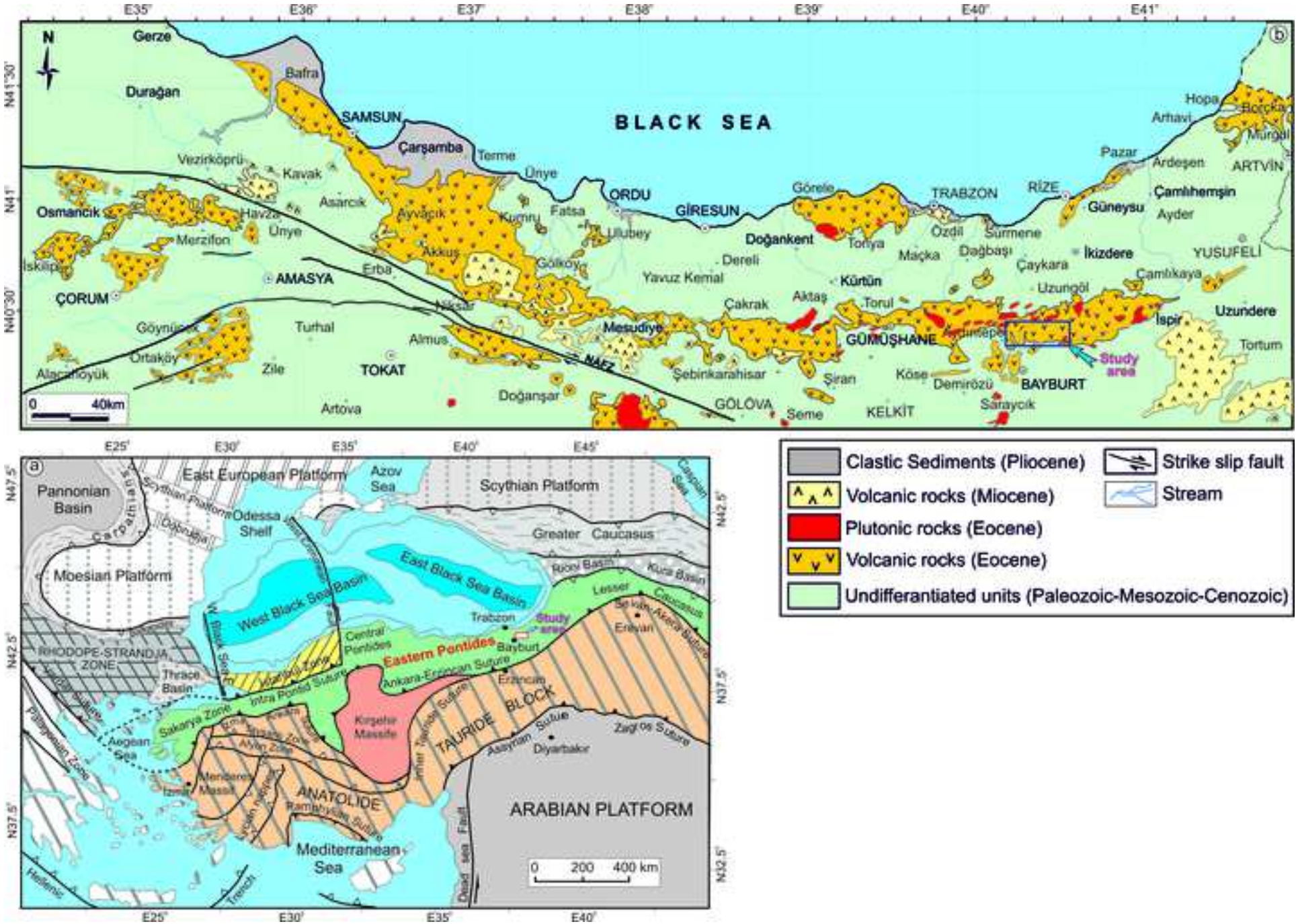

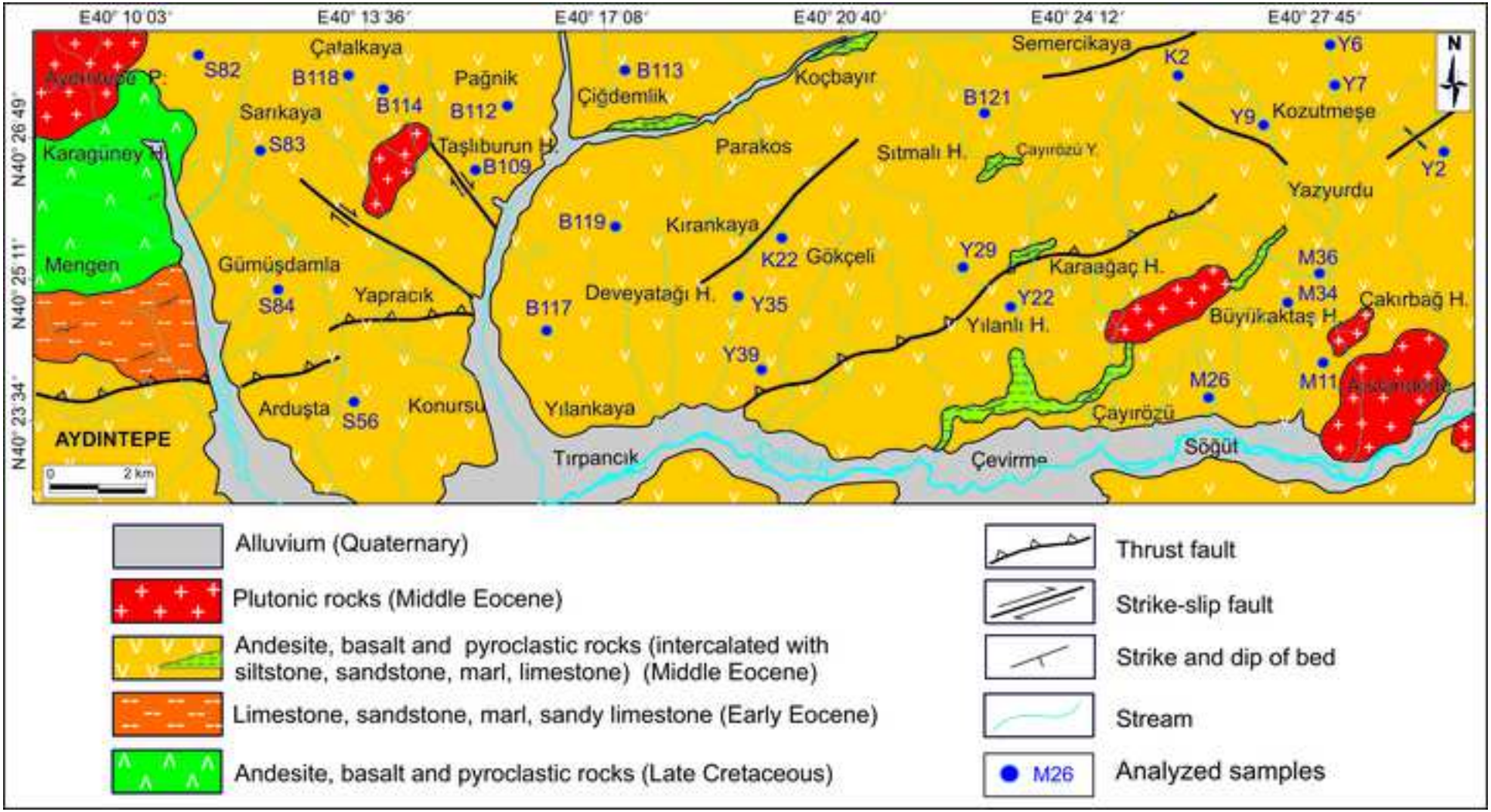

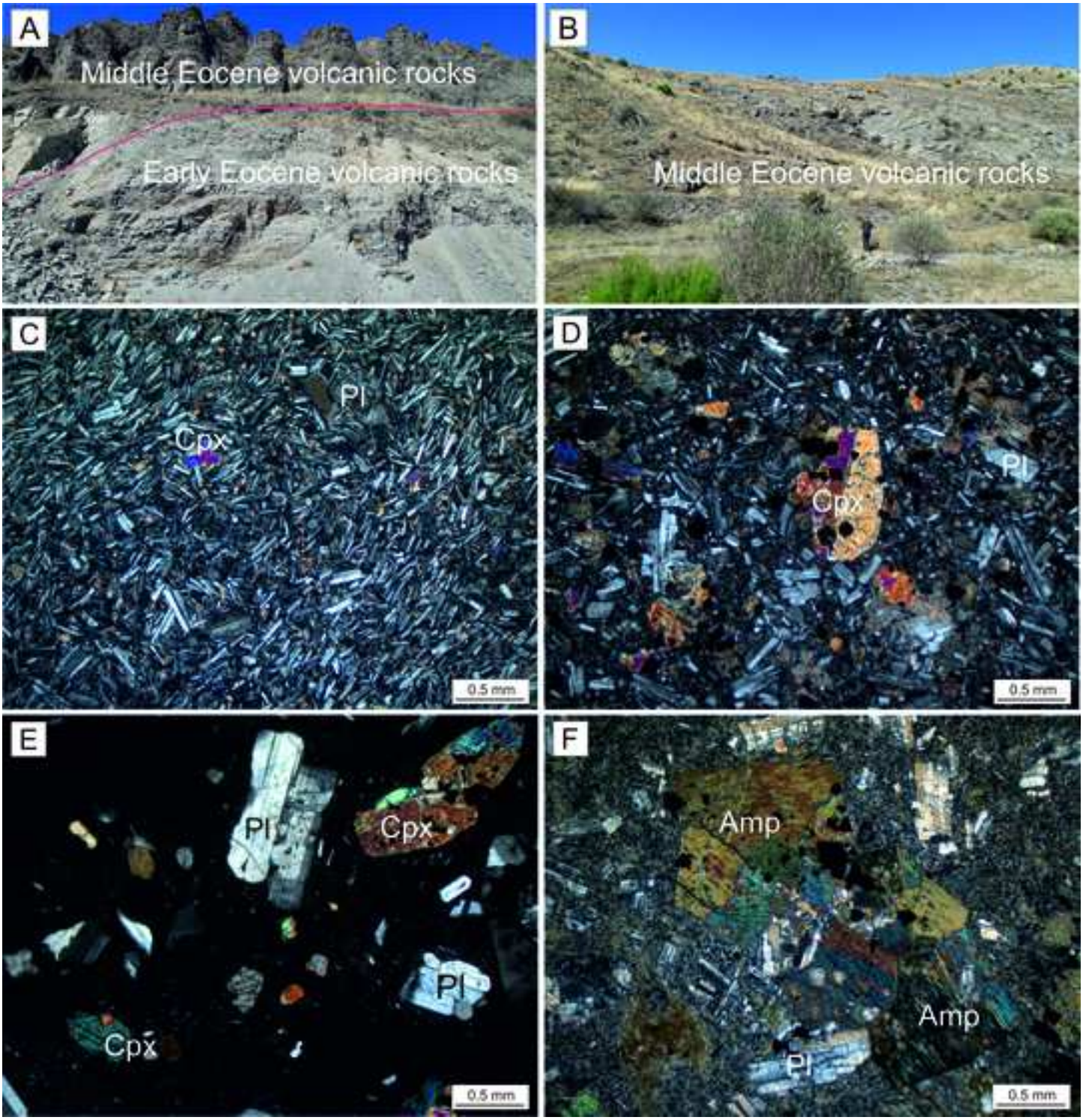

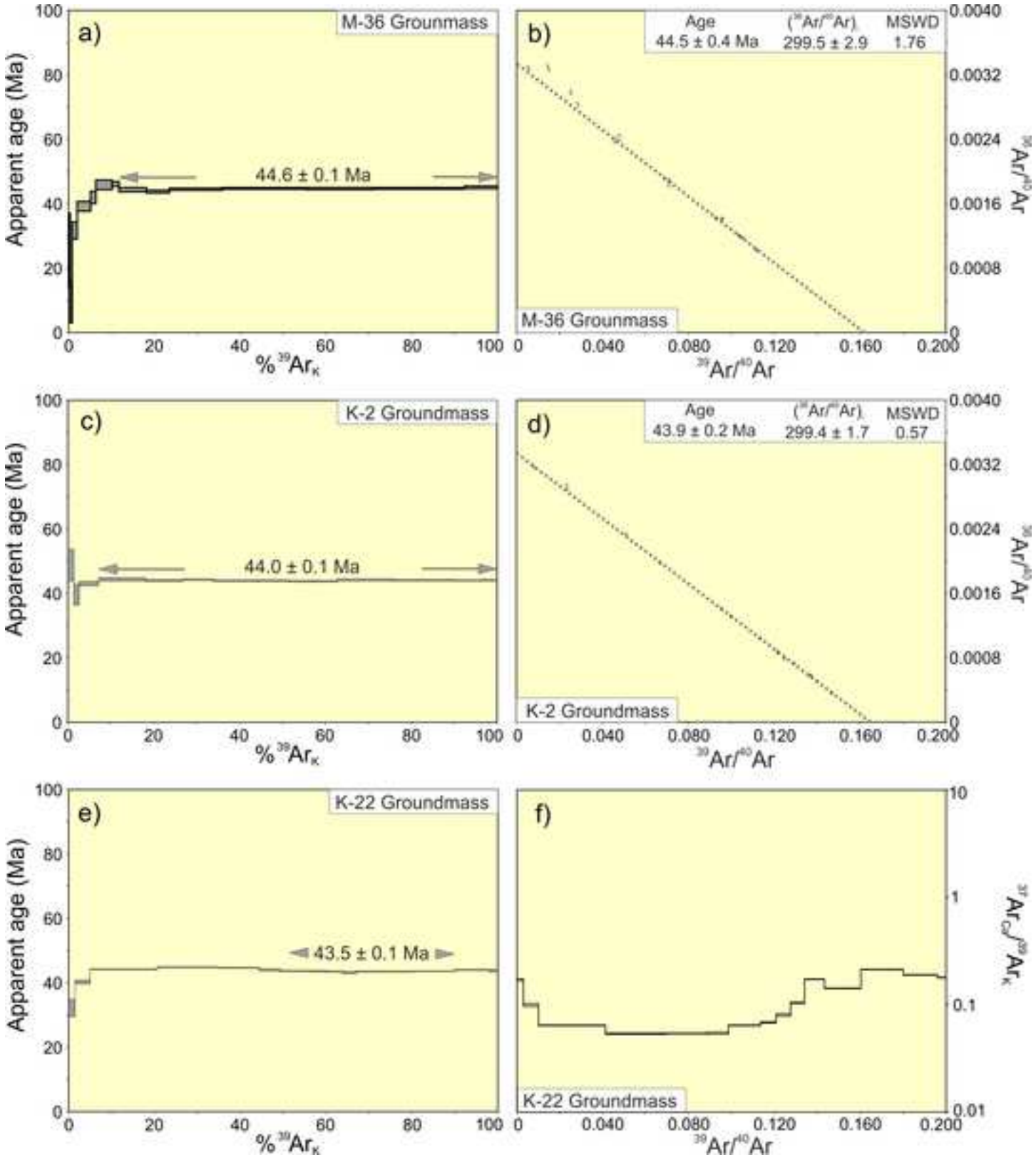

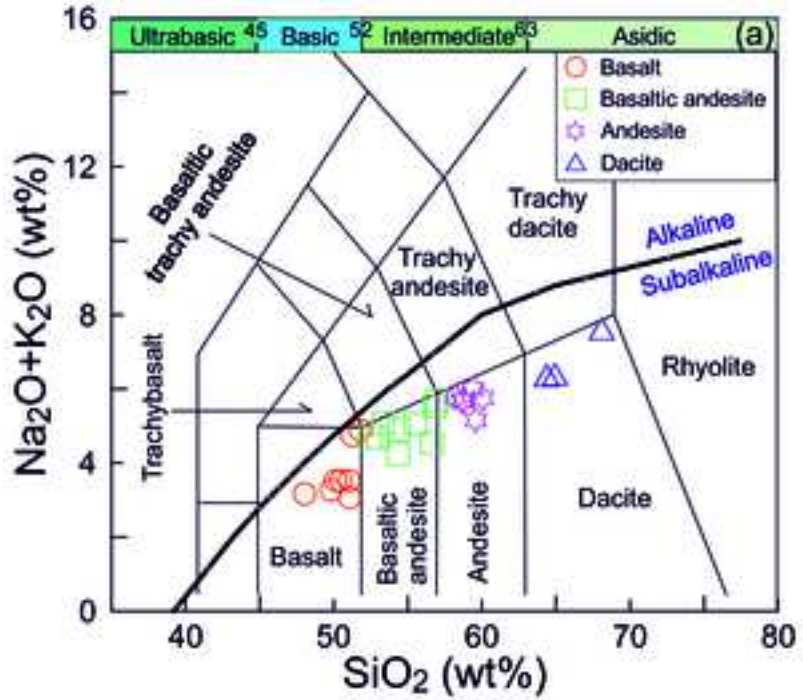

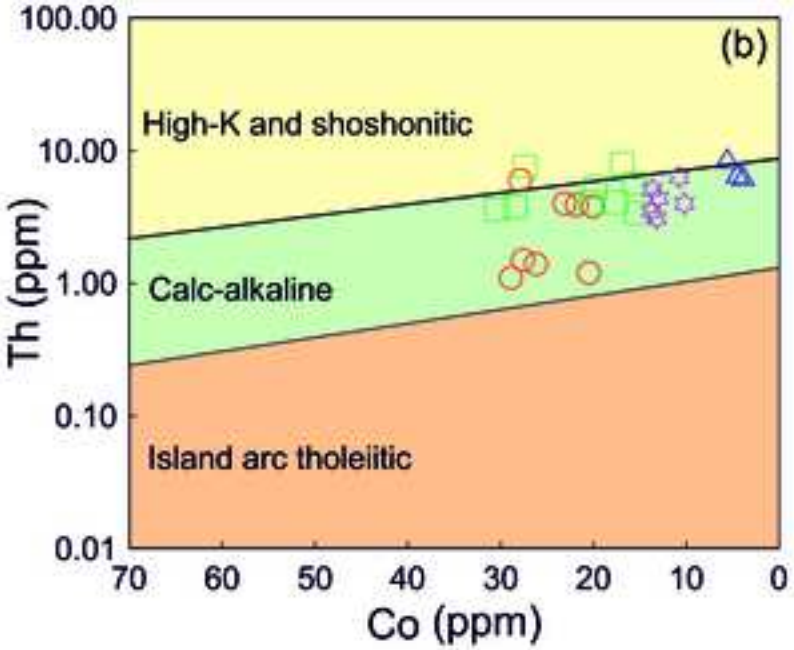

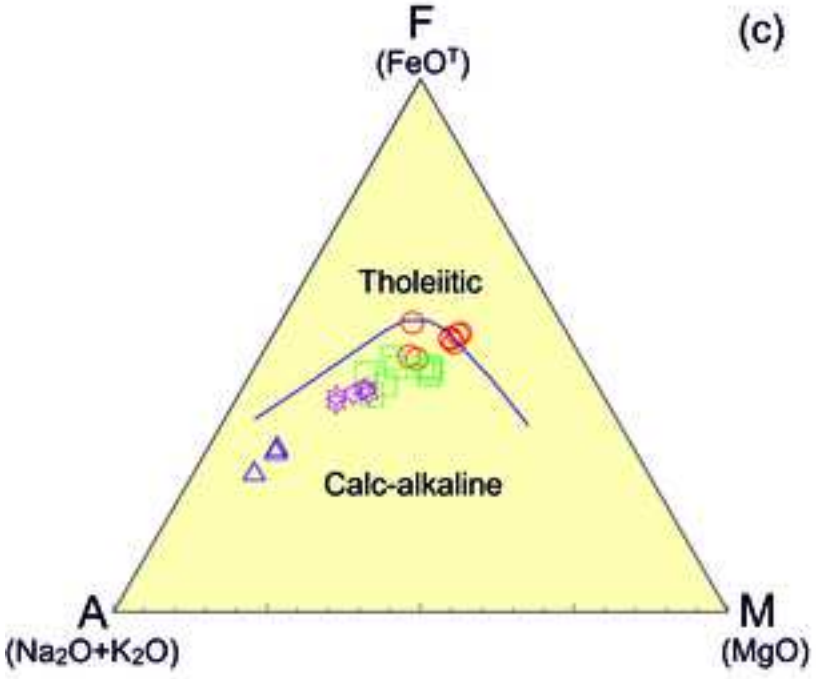

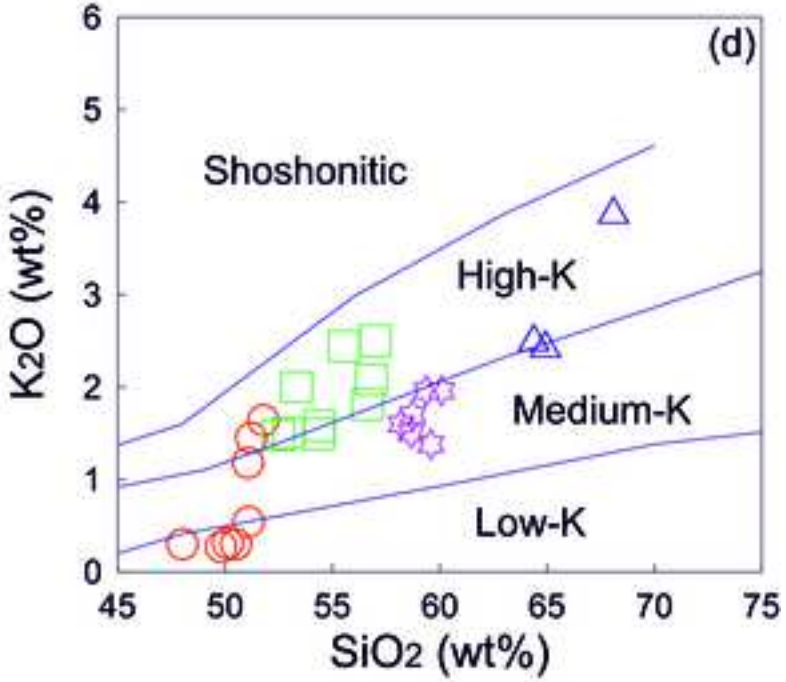

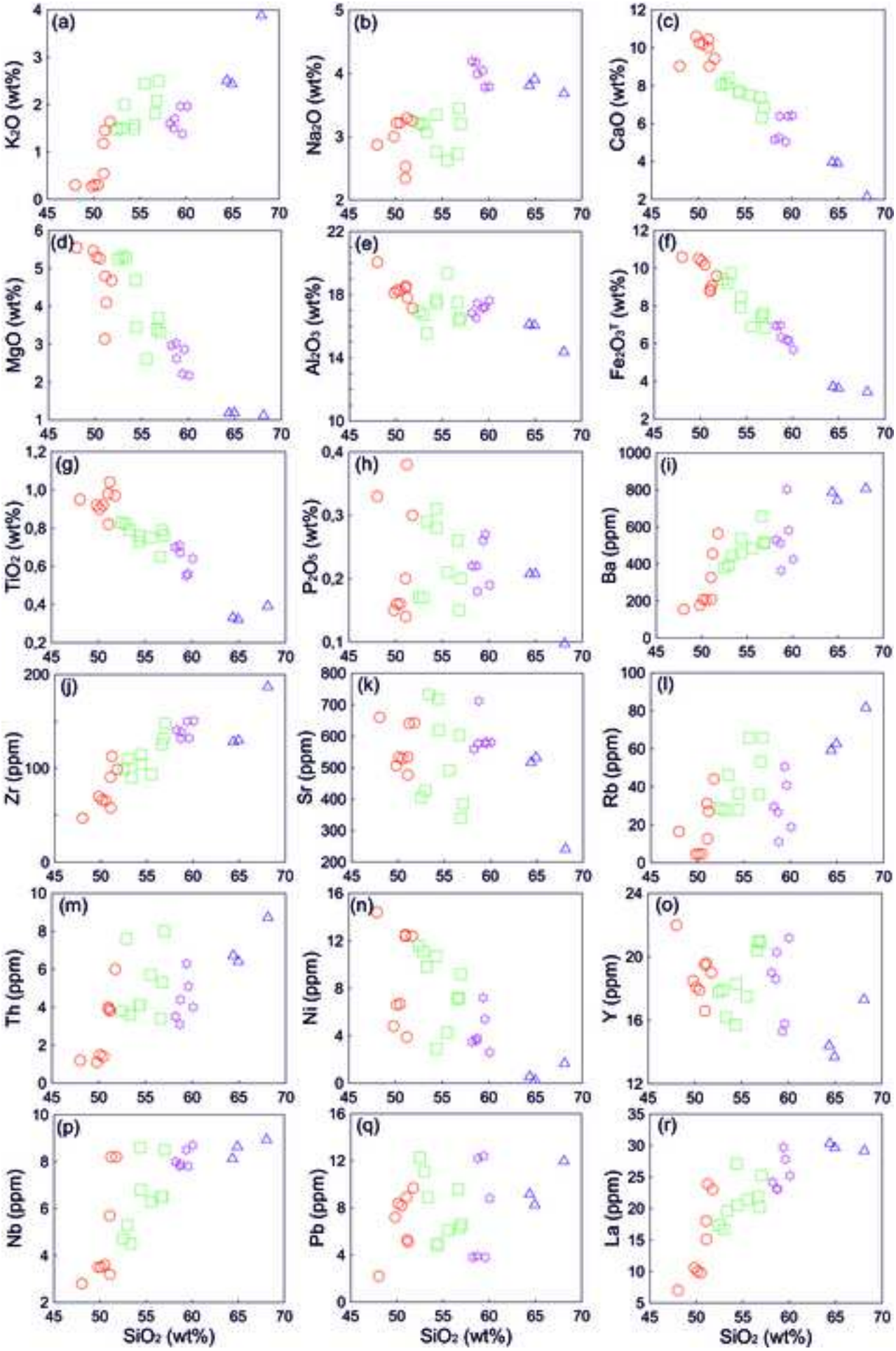

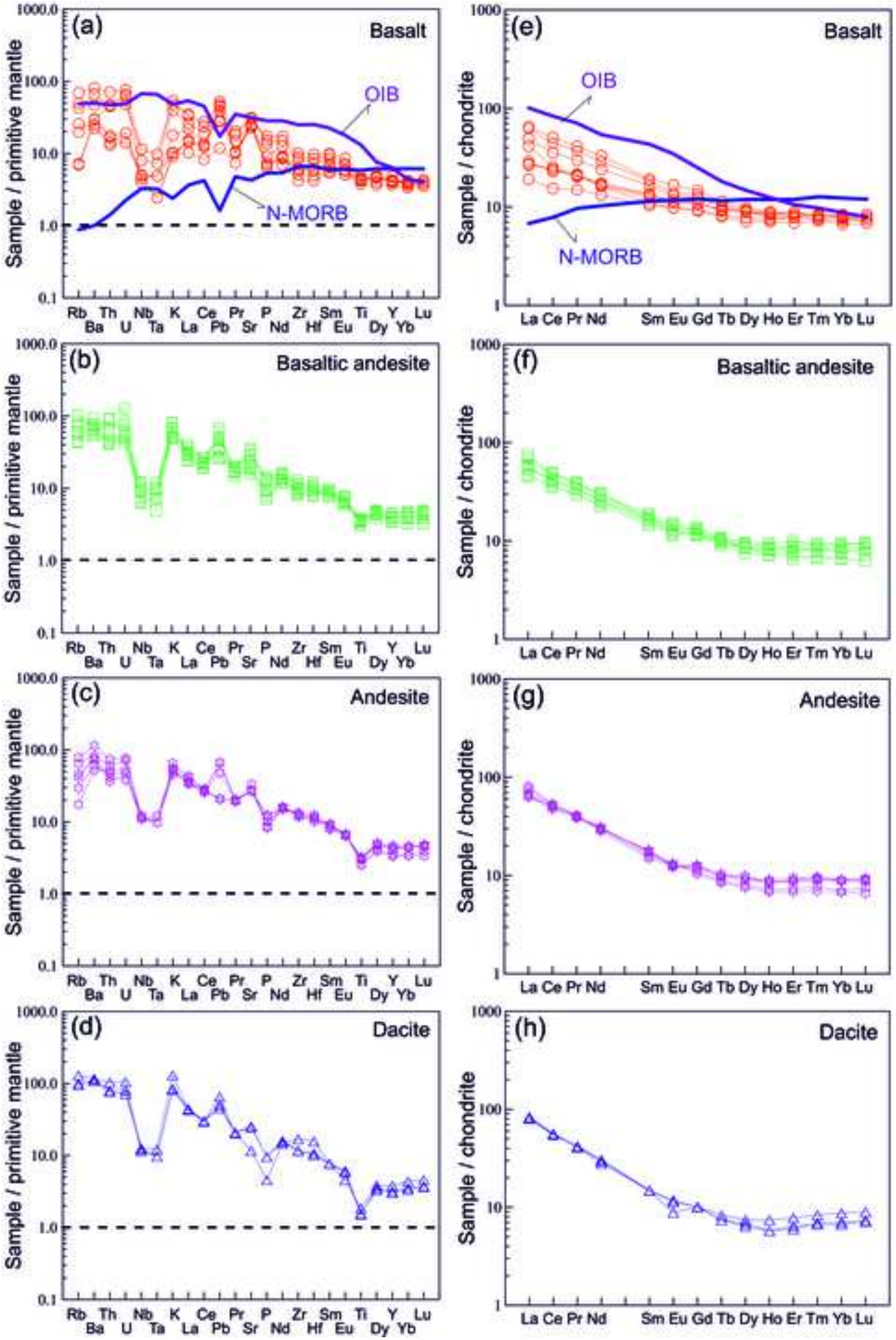

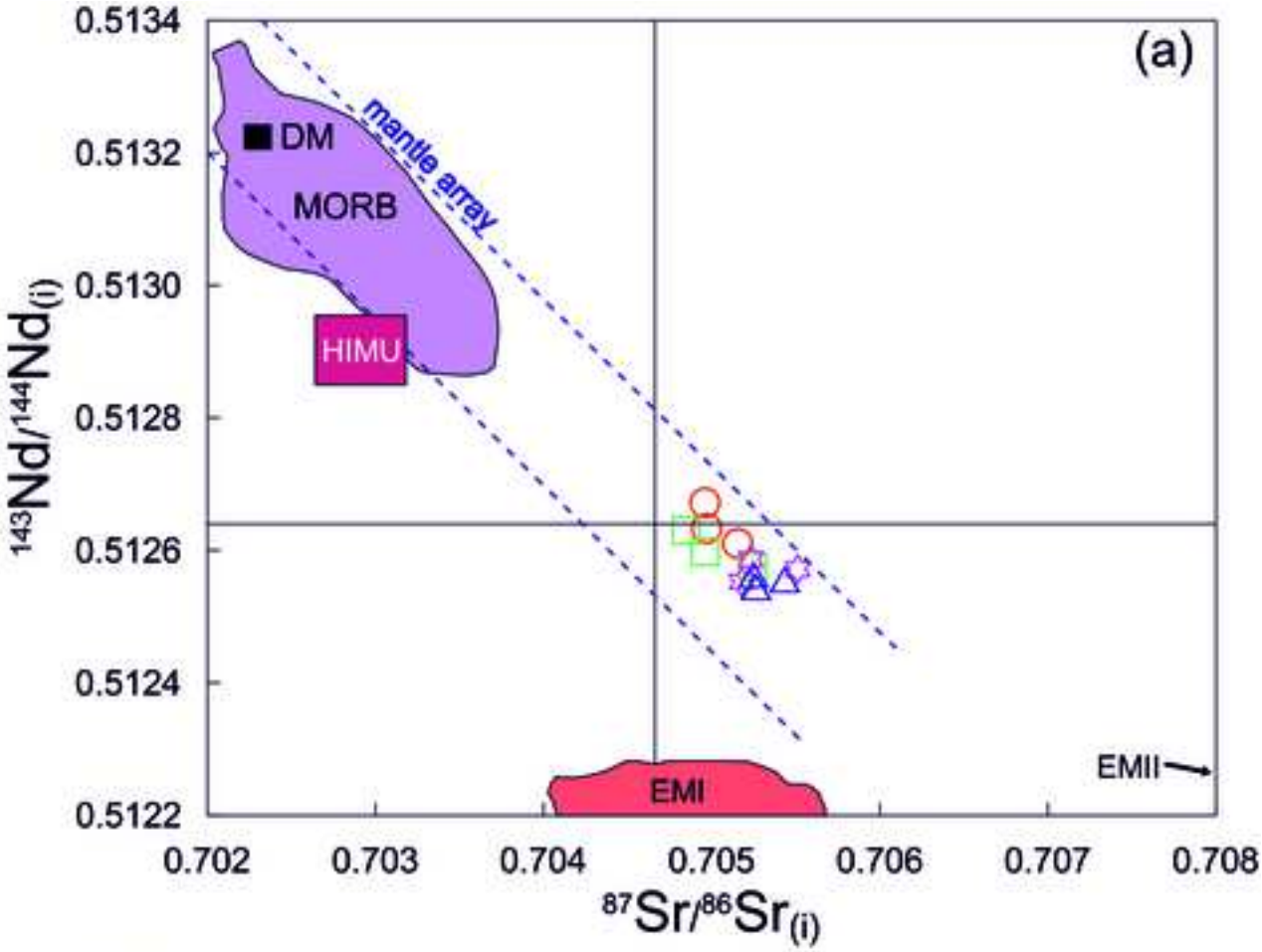

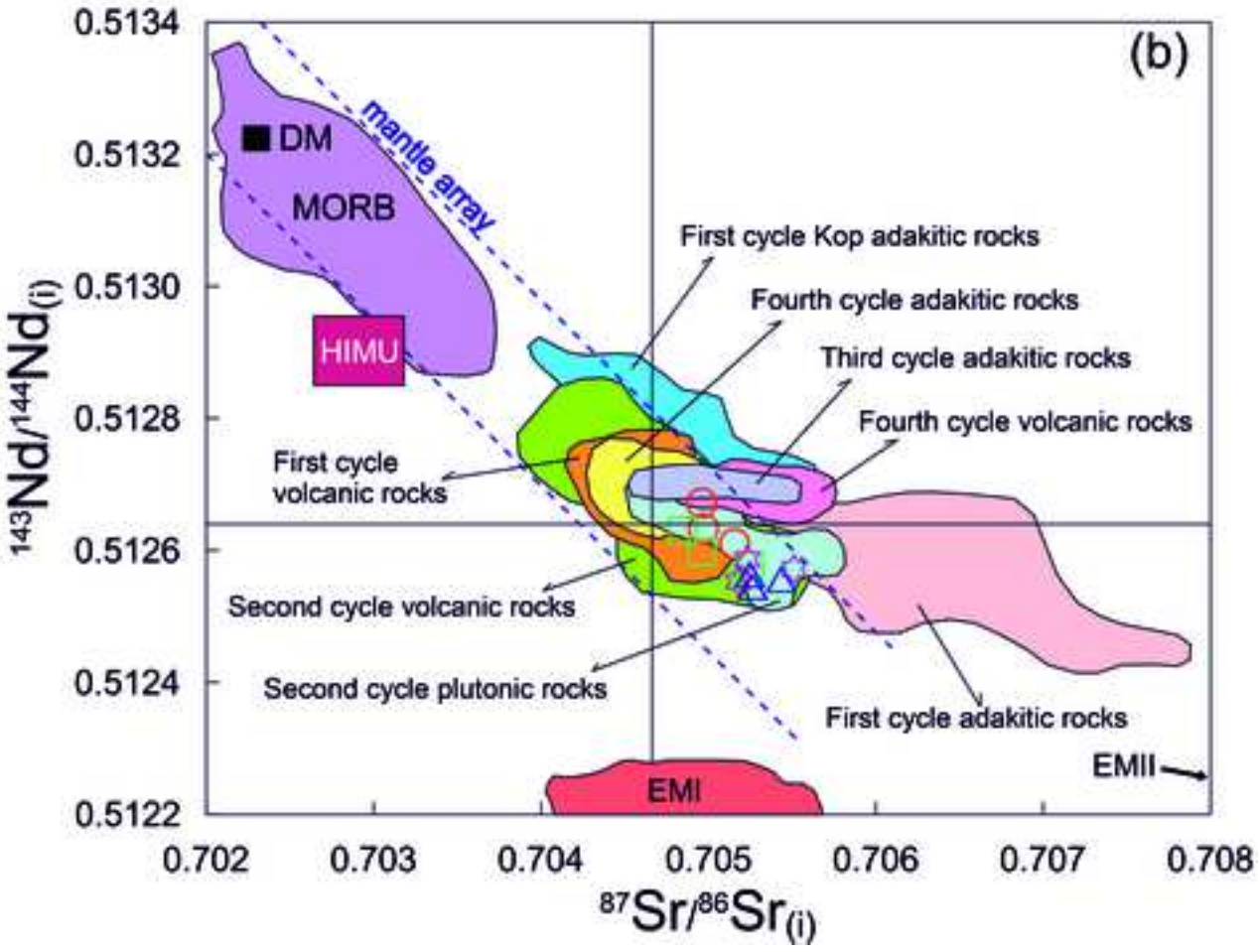

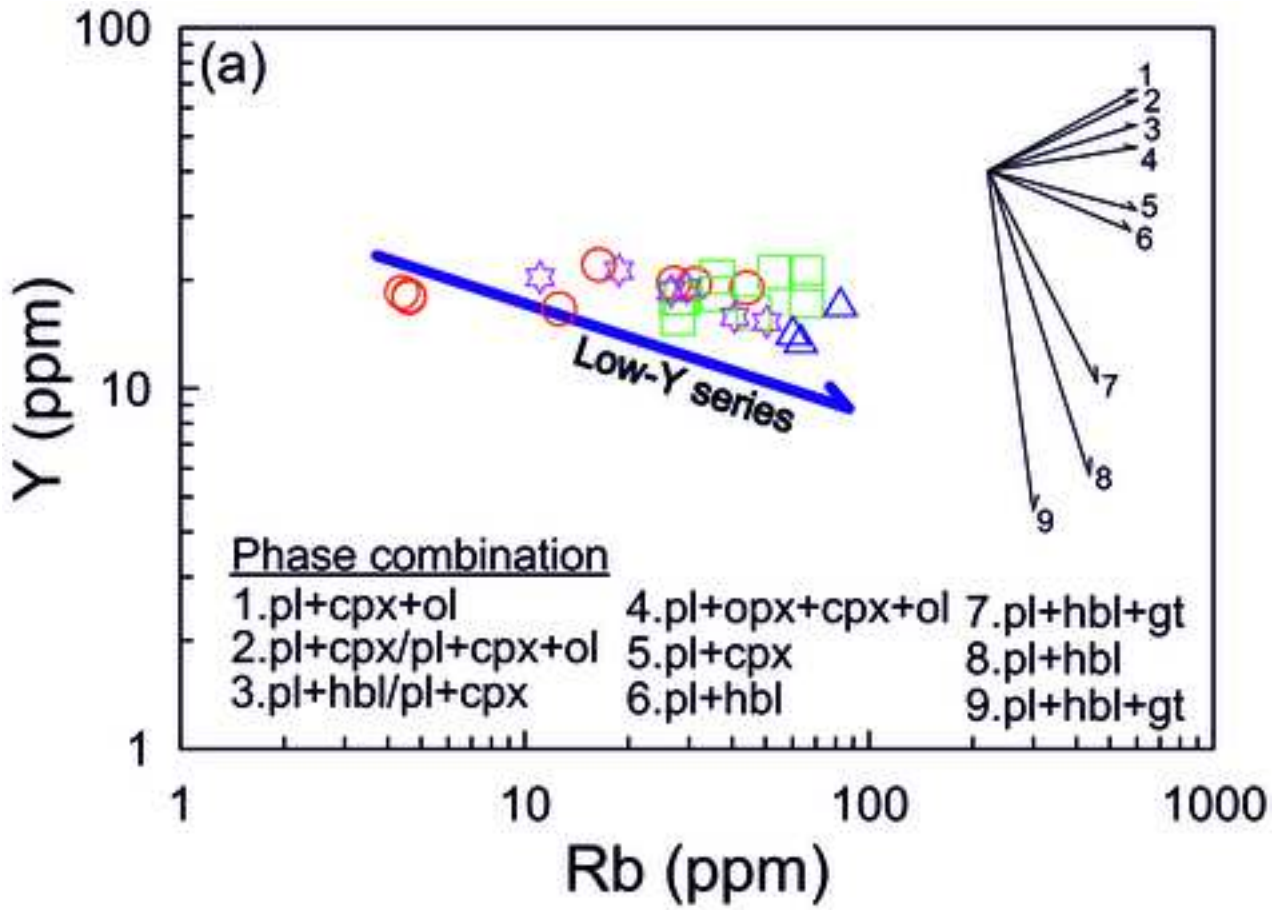

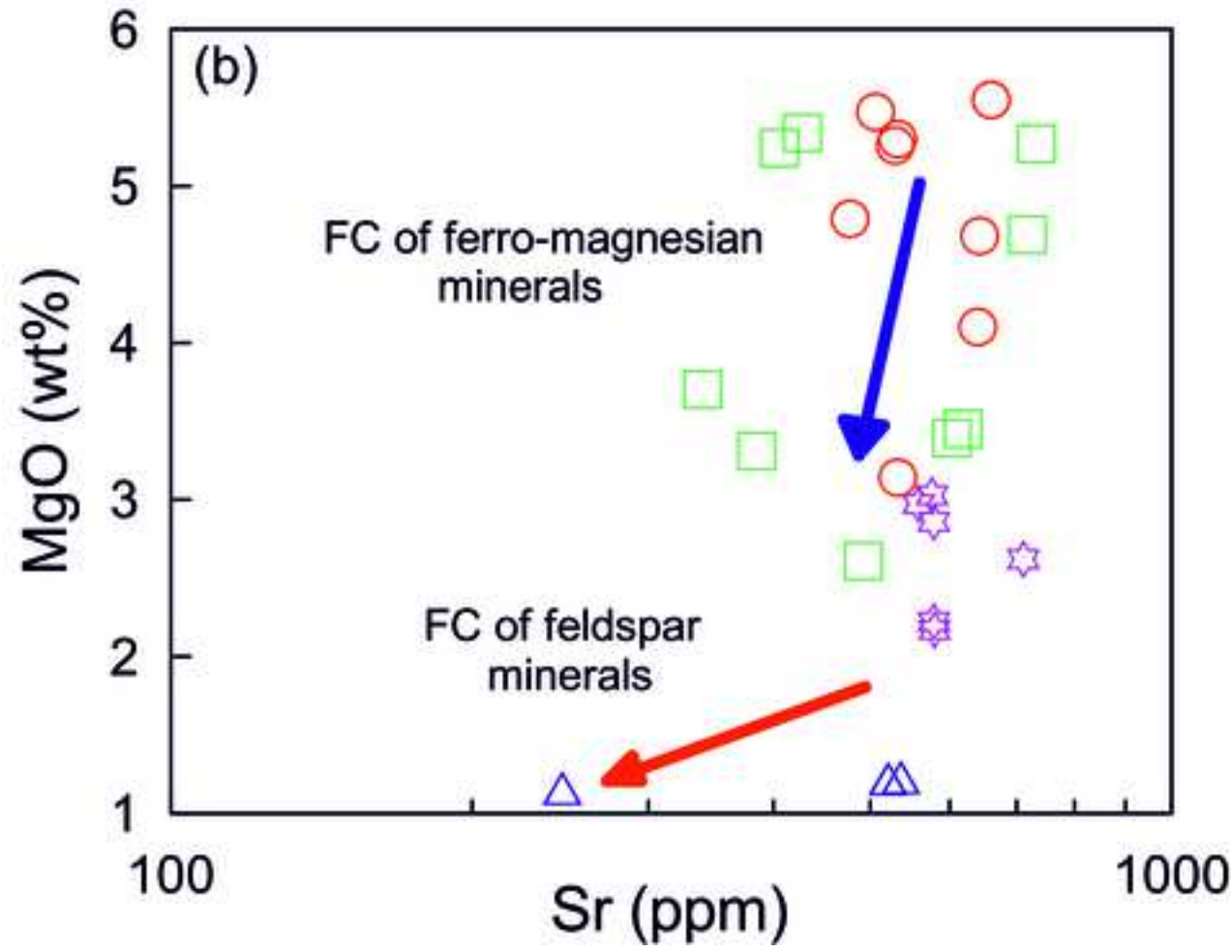

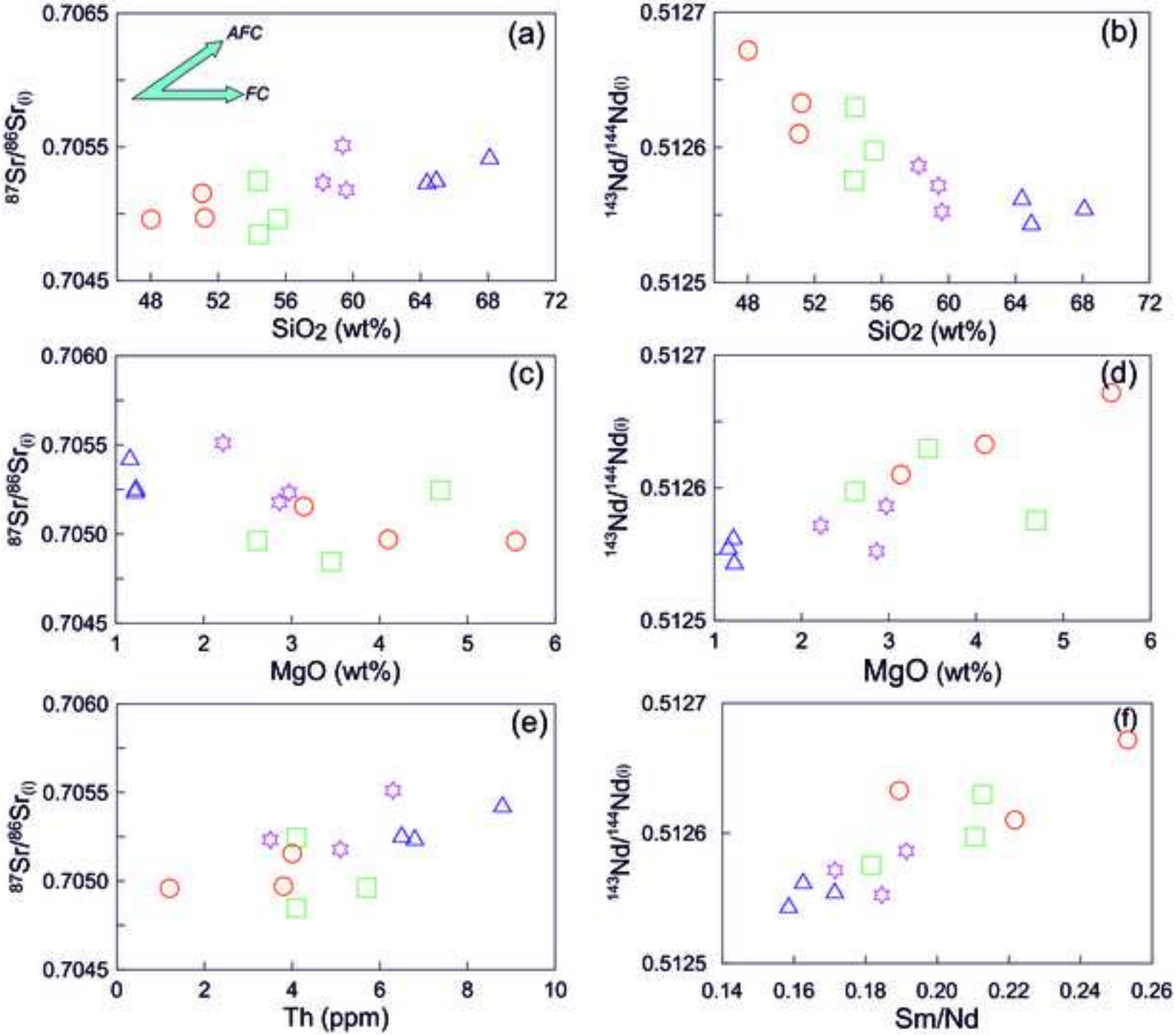

Colour Figure

Click here to access/download;Colour Figure;Figure 11.tif

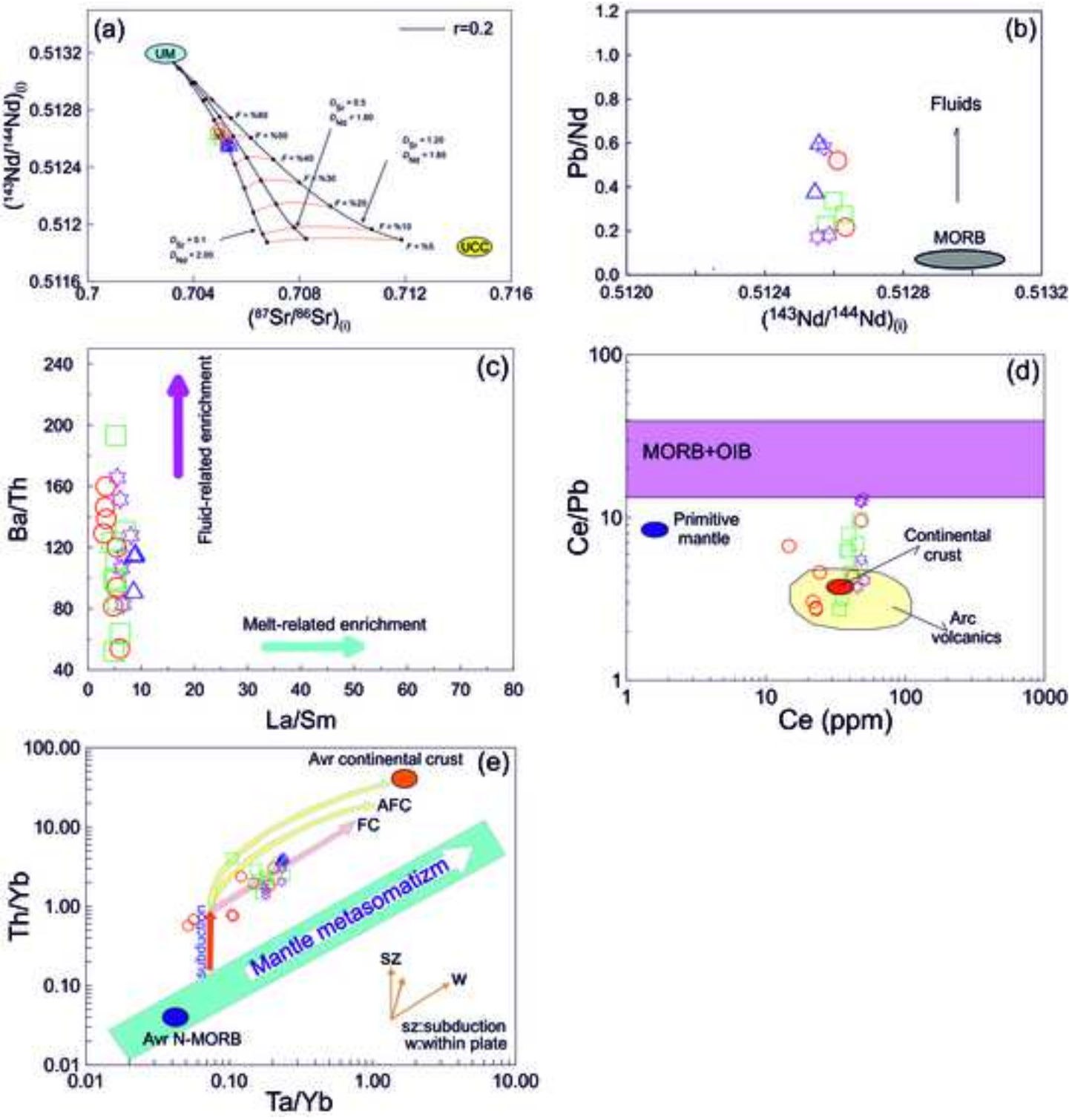

Tables and Captions

Table 1 ^{40}Ar-^{39}Ar dating results and locations of three samples for Bayburt volcanic rocks

Sample number	Material	Locality	Rock name	Plateau age (Ma)	± σ	Method
M-36	groundmass	Güvenli hill	basalt	44.6	0.1	$^{40}Ar/^{39}Ar$
K-2	groundmass	Yazyurdu hill	basaltic andesite	44.0	0.1	$^{40}Ar/^{39}Ar$
K-22	groundmass	Buğdaykabanı hill	dacite	43.5	0.1	$^{40}Ar/^{39}Ar$

Table 2 Major and trace elements compositions for Bayburt volcanic rocks

	Basalt								Basaltic andesite				
Sample	Y2	S82	S83	S84	Y7	S56	M36	M11	B117	B118	M26	M34	Y9
Major oxides (wt%)													
SiO_2	48.02	49.82	50.14	50.50	51.06	51.08	51.22	51.78	52.50	52.96	53.33	54.36	54.40
TiO_2	0.95	0.92	0.90	0.92	0.98	0.82	1.04	0.97	0.83	0.82	0.79	0.73	0.76
Al_2O_3	20.06	18.11	18.29	18.25	18.43	18.54	17.81	17.13	16.92	16.72	15.55	17.69	17.45
Fe_2O_{3T}	10.59	10.51	10.39	10.17	8.76	8.88	9.06	9.60	9.40	9.19	9.72	7.93	8.47
MnO	0.14	0.21	0.21	0.21	0.14	0.15	0.24	0.15	0.17	0.17	0.21	0.16	0.17
MgO	5.55	5.47	5.30	5.26	3.14	4.79	4.10	4.68	5.24	5.34	5.27	4.69	3.45
CaO	9.03	10.61	10.25	10.20	10.02	10.44	9.03	9.44	8.05	8.14	8.41	7.73	7.62
Na_2O	2.87	3.00	3.22	3.22	2.34	2.53	3.29	3.25	3.21	3.19	3.07	2.76	3.34
K_2O	0.30	0.27	0.31	0.30	1.18	0.54	1.45	1.64	1.48	1.50	2.00	1.49	1.58
P_2O_5	0.33	0.15	0.16	0.16	0.20	0.14	0.38	0.30	0.17	0.17	0.29	0.31	0.28
LOI	2.10	0.70	0.50	0.50	3.50	1.80	2.10	0.70	1.80	1.50	1.00	1.90	2.20
Total	99.94	99.77	99.67	99.69	99.75	99.71	99.72	99.64	99.77	99.70	99.64	99.75	99.72
Trace elements (ppm)													
Co	20.50	28.90	27.60	26.20	23.10	21.80	20.10	27.90	28.40	27.40	30.40	20.30	17.60
Ni	14.40	4.80	6.60	6.70	12.40	12.50	3.90	12.40	11.60	11.10	9.80	10.70	2.90
V	314.00	292.00	302.00	301.00	257.00	264.00	226.00	260.00	235.00	234.00	260.00	165.00	160.00
Cu	183.30	49.70	45.30	45.10	78.00	458.20	35.20	51.90	76.10	72.30	30.40	33.70	52.30
Pb	2.20	7.20	8.40	8.20	8.90	5.30	5.10	9.70	12.30	11.10	8.90	4.80	5.00
Zn	41.00	22.00	31.00	30.00	61.00	12.00	26.00	44.00	43.00	37.00	17.00	46.00	50.00
W	0.90	0.50	0.50	0.50	0.70	1.40	0.50	0.70	0.50	0.50	0.50	0.50	0.50
Rb	16.40	4.40	4.60	4.60	31.20	12.60	27.10	44.10	28.60	27.60	46.20	27.90	36.30
Ba	155.00	176.00	208.00	205.00	326.00	210.00	456.00	565.00	378.00	395.00	444.00	536.00	461.00
Sr	660.20	506.20	532.90	529.10	532.90	477.10	640.30	643.20	405.60	427.50	732.00	717.50	618.90
Ta	0.10	0.10	0.20	0.20	0.30	0.20	0.40	0.40	0.30	0.20	0.30	0.40	0.40
Nb	2.80	3.50	3.50	3.60	5.70	3.20	8.20	8.20	4.70	5.30	4.50	8.60	6.80
Hf	1.30	1.90	1.80	1.80	2.30	1.50	3.00	2.60	2.80	3.20	2.50	2.80	2.50
Zr	47.00	70.00	66.40	65.70	90.50	57.70	113.10	99.20	98.90	110.60	90.60	114.80	104.40
Y	22.00	18.50	18.10	17.90	19.50	16.60	19.60	19.00	17.80	17.90	16.20	15.70	18.30
Th	1.20	1.10	1.50	1.40	4.00	3.90	3.80	6.00	3.80	7.60	3.60	4.10	4.10
U	0.40	0.30	0.40	0.30	1.40	1.30	1.00	1.60	0.90	1.10	1.10	1.10	1.20
Ga	17.90	15.80	15.90	15.10	17.90	16.50	18.40	16.60	14.70	15.00	14.10	16.60	16.70
La	7.00	10.60	10.00	9.80	18.00	15.10	23.90	23.00	17.40	16.70	19.60	27.10	20.50
Ce	14.70	21.90	23.00	22.90	33.80	24.40	48.50	42.30	33.70	35.20	41.00	46.90	39.40
Pr	2.04	2.89	2.94	2.78	4.08	2.84	5.62	5.08	4.09	4.09	5.07	5.39	4.72
Nd	9.40	12.40	11.60	12.00	17.10	11.50	23.50	20.50	17.10	15.90	21.90	21.20	18.20
Sm	2.38	3.14	2.89	3.06	3.79	2.51	4.45	4.25	3.56	3.38	4.34	3.85	3.87
Eu	0.86	0.95	1.01	1.00	1.14	0.85	1.45	1.21	1.01	1.00	1.33	1.14	1.26
Gd	2.86	3.30	3.34	3.35	3.79	2.79	4.49	4.12	3.59	3.61	4.17	3.49	3.74
Tb	0.48	0.55	0.53	0.54	0.58	0.46	0.66	0.61	0.58	0.56	0.58	0.53	0.59
Dy	2.94	3.38	3.48	3.47	3.40	2.70	3.72	3.56	3.29	3.25	3.24	2.85	3.41
Ho	0.63	0.72	0.64	0.68	0.73	0.60	0.76	0.74	0.70	0.62	0.61	0.61	0.71
Er	1.94	2.09	1.99	1.99	2.09	1.71	2.21	2.13	2.15	1.92	1.62	1.79	2.09
Tm	0.27	0.30	0.30	0.28	0.30	0.26	0.29	0.30	0.28	0.31	0.25	0.24	0.30
Yb	1.77	1.94	1.92	1.87	2.03	1.65	2.07	1.96	2.02	1.90	1.63	1.65	2.14
Lu	0.28	0.30	0.28	0.28	0.32	0.26	0.30	0.30	0.30	0.32	0.24	0.24	0.33
$(Eu/Eu^*)_n$	1.01	0.90	0.99	0.95	0.91	0.98	0.98	0.87	0.86	0.87	0.94	0.93	1.00
$(La/Lu)_n$	2.59	3.66	3.70	3.62	5.82	6.01	8.25	7.94	6.01	5.40	8.46	11.69	6.43
$(La/Sm)_n$	1.85	2.12	2.18	2.02	2.99	3.79	3.38	3.41	3.08	3.11	2.84	4.43	3.33
$(Gd/Lu)_n$	1.27	1.37	1.48	1.49	1.47	1.33	1.86	1.71	1.49	1.40	2.16	1.81	1.41
$(La/Yb)_n$	2.67	3.69	3.52	3.54	5.99	6.18	7.80	7.93	5.82	5.94	8.13	11.10	6.47
Mg#	53.57	53.40	52.90	53.24	44.11	54.29	49.91	51.77	55.10	56.13	54.41	56.56	47.28
Ce/Pb	6.68	3.04	2.74	2.79	3.80	4.60	9.51	4.36	2.74	3.17	4.61	9.77	7.88
Nb/La	0.40	0.33	0.35	0.37	0.32	0.21	0.34	0.36	0.27	0.32	0.23	0.32	0.33
Ba/La	22.14	16.60	20.80	20.92	18.11	13.91	19.08	24.57	21.72	23.65	22.65	19.78	22.49
Dy/Yb	1.66	1.74	1.81	1.86	1.67	1.64	1.80	1.82	1.63	1.71	1.99	1.73	1.59
Pb/Ce	0.15	0.33	0.37	0.36	0.26	0.22	0.11	0.23	0.36	0.32	0.22	0.10	0.13
Th/Ce	0.08	0.05	0.07	0.06	0.12	0.16	0.08	0.14	0.11	0.22	0.09	0.09	0.10

Table 2'continued

	Basaltic andesite				Andesite						Dacite		
Sample	Y6	B119	B109	K2	B113	B114	B112	Y29	Y22	B121	Y35	Y39	K22
Major oxides (wt%)													
SiO_2	55.54	56.63	56.82	57.00	58.21	58.67	58.75	59.39	59.59	60.07	64.38	64.93	68.10
TiO_2	0.75	0.65	0.79	0.76	0.70	0.71	0.67	0.55	0.56	0.64	0.34	0.33	0.40
Al_2O_3	19.35	17.51	16.36	16.53	16.84	16.53	17.44	17.14	17.23	17.63	16.22	16.16	14.48
Fe_2O_{3T}	6.90	7.44	7.61	6.84	6.94	6.97	6.35	6.19	6.16	5.67	3.81	3.71	3.52
MnO	0.12	0.17	0.13	0.10	0.14	0.14	0.13	0.11	0.16	0.12	0.14	0.14	0.06
MgO	2.61	3.39	3.70	3.31	2.97	3.03	2.62	2.22	2.86	2.17	1.22	1.23	1.16
CaO	7.50	7.40	6.32	6.86	5.15	5.25	6.39	5.04	6.39	6.43	4.05	3.99	2.22
Na_2O	2.62	2.73	3.45	3.20	4.19	4.17	3.99	4.04	3.78	3.79	3.83	3.93	3.71
K_2O	2.44	1.81	2.08	2.50	1.60	1.50	1.70	1.96	1.38	1.96	2.54	2.47	3.92
P_2O_5	0.21	0.26	0.15	0.20	0.22	0.22	0.18	0.26	0.27	0.19	0.21	0.21	0.10
LOI	1.70	1.70	2.30	2.50	2.80	2.50	1.50	2.90	1.40	1.10	3.10	2.70	2.10
Total	99.74	99.69	99.71	99.80	99.76	99.69	99.72	99.80	99.78	99.77	99.84	99.80	99.77
Trace elements (ppm)													
Co	15.60	15.40	19.80	16.90	13.80	13.20	13.00	10.80	13.70	10.20	4.50	3.90	5.60
Ni	4.30	7.10	7.20	9.20	3.50	3.60	3.80	7.20	5.40	2.60	0.70	0.40	1.80
V	156.00	143.00	185.00	163.00	140.00	150.00	145.00	87.00	111.00	117.00	40.00	40.00	50.00
Cu	72.10	42.20	63.40	39.60	25.60	24.00	46.30	32.60	30.90	29.20	3.50	2.50	9.40
Pb	6.10	9.60	6.30	6.60	3.80	3.90	12.20	12.40	3.80	8.80	9.30	8.40	12.10
Zn	37.00	44.00	49.00	33.00	32.00	36.00	48.00	56.00	45.00	48.00	63.00	60.00	23.00
W	0.90	0.50	0.50	1.10	0.50	0.50	0.50	0.70	0.70	0.50	5.30	0.80	0.50
Rb	65.80	36.10	53.20	65.90	29.50	26.60	11.10	50.60	40.80	18.80	60.10	63.40	82.50
Ba	484.00	657.00	518.00	511.00	530.00	514.00	364.00	805.00	583.00	425.00	796.00	753.00	816.00
Sr	492.20	603.10	339.80	385.20	559.00	576.30	711.70	578.90	578.60	579.60	521.20	536.80	246.10
Ta	0.30	0.40	0.40	0.50	0.40	0.40	0.50	0.40	0.40	0.40	0.40	0.40	0.50
Nb	6.30	6.50	6.50	8.50	8.00	7.80	7.90	8.50	7.80	8.70	8.20	8.70	9.00
Hf	2.40	3.10	3.50	3.80	3.50	3.40	3.60	3.40	3.10	3.90	3.10	3.30	4.90
Zr	93.60	125.50	132.30	147.90	141.00	131.70	139.00	150.00	132.20	150.80	130.00	131.70	188.70
Y	17.50	20.40	21.00	20.90	19.00	18.60	20.30	15.30	15.80	21.20	14.50	13.80	17.40
Th	5.70	3.40	5.30	8.00	3.50	3.10	4.40	6.30	5.10	4.00	6.80	6.50	8.80
U	1.60	1.00	1.80	2.70	0.80	1.00	1.10	1.60	1.50	1.00	1.70	1.50	2.20
Ga	16.90	14.40	15.00	13.80	13.30	12.70	14.50	15.90	16.60	15.10	15.00	14.70	13.00
La	21.40	21.90	20.20	25.30	24.20	23.10	23.10	29.70	27.80	25.20	30.60	29.90	29.40
Ce	38.10	47.90	39.50	45.50	47.60	48.70	45.40	51.20	50.20	48.40	54.10	53.30	52.50
Pr	4.52	5.36	4.71	5.33	5.51	5.38	5.27	5.65	5.57	5.42	5.73	5.78	5.57
Nd	18.10	21.00	18.60	19.80	20.90	21.60	20.20	21.40	22.00	21.10	21.10	21.70	19.90
Sm	3.81	4.13	3.80	4.15	4.00	4.18	3.48	3.67	4.06	3.97	3.43	3.44	3.41
Eu	1.09	1.24	0.99	1.07	1.06	1.11	1.08	1.15	1.12	1.09	1.03	0.98	0.77
Gd	3.61	4.02	3.93	4.21	3.90	3.85	3.63	3.19	3.41	3.79	3.07	3.11	3.11
Tb	0.53	0.60	0.62	0.63	0.60	0.60	0.57	0.49	0.51	0.55	0.43	0.43	0.48
Dy	3.23	3.55	3.68	3.64	3.42	3.75	3.77	2.86	3.05	3.51	2.43	2.60	2.84
Ho	0.68	0.74	0.78	0.81	0.77	0.75	0.70	0.58	0.61	0.72	0.49	0.49	0.63
Er	1.96	2.18	2.53	2.36	2.36	2.16	2.17	1.69	1.82	2.25	1.61	1.49	1.95
Tm	0.29	0.33	0.33	0.34	0.34	0.32	0.33	0.25	0.28	0.35	0.24	0.25	0.30
Yb	1.95	2.38	2.24	2.27	2.22	2.22	2.15	1.68	1.71	2.27	1.65	1.75	2.16
Lu	0.28	0.35	0.36	0.37	0.34	0.33	0.35	0.25	0.29	0.36	0.28	0.27	0.34
$(Eu/Eu^*)_n$	0.89	0.92	0.78	0.78	0.81	0.83	0.92	1.00	0.90	0.85	0.95	0.90	0.71
$(La/Lu)_n$	7.91	6.48	5.81	7.08	7.37	7.25	6.83	12.30	9.93	7.25	11.32	11.47	8.95
$(La/Sm)_n$	3.54	3.34	3.35	3.84	3.81	3.48	4.18	5.09	4.31	4.00	5.62	5.47	5.43
$(Gd/Lu)_n$	1.60	1.43	1.36	1.41	1.42	1.45	1.29	1.58	1.46	1.31	1.36	1.43	1.14
$(La/Yb)_n$	7.42	6.22	6.09	7.53	7.37	7.03	7.26	11.95	10.99	7.50	12.53	11.55	9.20
Mg#	45.44	50.08	51.70	51.58	48.51	48.90	47.60	44.12	50.55	45.73	41.35	42.19	42.05
Ce/Pb	6.25	4.99	6.27	6.89	12.53	12.49	3.72	4.13	13.21	5.50	5.82	6.35	4.34
Nb/La	0.29	0.30	0.32	0.34	0.33	0.34	0.34	0.29	0.28	0.35	0.27	0.29	0.31
Ba/La	22.62	30.00	25.64	20.20	21.90	22.25	15.76	27.10	20.97	16.87	26.01	25.18	27.76
Dy/Yb	1.66	1.49	1.64	1.60	1.54	1.69	1.75	1.70	1.78	1.55	1.47	1.49	1.31
Pb/Ce	0.16	0.20	0.16	0.15	0.08	0.08	0.27	0.24	0.08	0.18	0.17	0.16	0.23
Th/Ce	0.15	0.07	0.13	0.18	0.07	0.06	0.10	0.12	0.10	0.08	0.13	0.12	0.17

Fe_2O_{3T} is total iron as Fe_2O_3, LOI is loss on ignition, Mg# (Mg number) = molar $100\times MgO/(MgO + Fe_2O_{3T})$, Eu*= (Sm + Gd)n/2

Table 3 Sr-Nd isotope compositions for Bayburt volcanic rocks

Sample	Rb (ppm)	Sr (ppm)	$^{87}Rb/^{86}Sr$	$^{87}Sr/^{86}Sr$	(2σ)	$^{87}Sr^{86}Sr_{(i)}$	Sm (ppm)	Nd (ppm)	$^{147}Sm/^{144}Nd$	$^{143}/^{144}Nd$	(2σ)	$^{143}Nd/^{144}Nd_{(i)}$	$\varepsilon Nd_{(i)}$[a]	T_{DM}[b]	T_{DM}[c]
Basalt															
Y2	16.40	660.20	0.0720	0.705004	10	0.704959	2.38	9.40	0.153069	0.512716	5	0.512672	1.76	1.01	0.71
Y7	31.20	532.90	0.1698	0.705261	10	0.705154	3.79	17.10	0.133993	0.512649	4	0.512610	0.56	0.90	0.81
M36	27.10	640.30	0.1227	0.705047	9	0.704971	4.45	23.50	0.114481	0.512666	5	0.512633	1.00	0.71	0.77
Basaltic andesite															
M34	27.90	717.50	0.1128	0.705316	9	0.705245	3.85	21.20	0.109790	0.512607	5	0.512575	-0.11	0.76	0.86
Y9	36.30	618.90	0.1701	0.704953	11	0.704847	3.87	18.20	0.128552	0.512667	5	0.512630	0.94	0.82	0.78
Y6	65.80	492.20	0.3877	0.705205	10	0.704963	3.81	18.10	0.127258	0.512634	4	0.512597	0.31	0.86	0.83
Andesite															
B113	29.50	559.00	0.1530	0.705328	9	0.705233	4.00	20.90	0.115705	0.512620	5	0.512586	0.10	0.78	0.85
Y29	50.60	578.90	0.2535	0.705669	10	0.705511	3.67	21.40	0.103679	0.512601	5	0.512572	-0.19	0.73	0.87
Y22	40.80	578.60	0.2045	0.705305	10	0.705177	4.06	22.00	0.111569	0.512584	5	0.512552	-0.57	0.80	0.90
Dacite															
Y35	60.10	521.20	0.3344	0.705457	10	0.705248	3.43	21.10	0.098277	0.512592	5	0.512564	-0.35	0.71	0.88
Y39	63.40	536.80	0.3425	0.705478	10	0.705264	3.44	21.70	0.095838	0.512573	5	0.512545	-0.71	0.72	0.91
K22	82.50	246.10	0.9722	0.706042	10	0.705434	3.41	19.90	0.103595	0.512586	5	0.512556	-0.49	0.75	0.90

[a] $\varepsilon Nd_{(i)}$ values are calculated based on present-day $^{147}Sm/^{144}Nd=0.1967$ and $^{143}Nd/^{144}Nd=0.512638$

[b] Single stage model age (T_{DM}[b]) calculated with depleted mantle present-day parameters $^{143}Nd/^{144}Nd=0.513151$ and $^{147}Sm/^{144}Nd=0.219$

[c] Two-stage model age (T_{DM}[c]) according to Liew and Hofman (1988)

The Initial $^{143}Nd/^{144}Nd$ and $^{87}Sr/^{86}Sr$ ratios were calculated based on the $^{40}Ar–^{39}Ar$ ages reported in Table 1

Supplementary Tables

Table S1 ^{40}Ar-^{39}Ar dating results for Bayburt volcanic rocks

Step / Sample	^{40}Ar	Error ^{40}Ar	^{39}Ar	Error ^{39}Ar	^{38}Ar	Error ^{38}Ar	^{37}Ar	Error ^{37}Ar	^{36}Ar	Error ^{36}Ar	$^{40}Ar^*/^{39}Ar_K$	Error $^{40}Ar^*/^{39}Ar_K$	Apparent age (Ma)	Error Age (Ma)	Delay to irradiation (day)
M36															
1	2030.403	5.886	11.426	0.042	0.0000010	0.0064	2.079	0.017	6.939	0.048	3.510	1.611	25.46	11.60	129.65
2	881.187	6.138	13.221	0.058	0.0000010	0.0074	2.046	0.028	3.017	0.030	1.299	0.879	9.46	6.39	129.67
3	1051.965	6.103	26.718	0.247	0.0000010	0.0102	4.484	0.025	3.278	0.020	4.377	0.371	31.69	2.66	129.69
4	2889.516	2.059	83.278	0.056	0.0000010	0.0110	17.527	0.110	8.580	0.039	5.414	0.213	39.12	1.53	129.71
5	706.199	4.839	34.045	0.321	0.0049210	0.0061	6.567	0.041	1.805	0.023	5.805	0.266	41.91	1.90	129.74
6	2196.906	5.599	100.862	0.322	0.0033680	0.0099	22.049	0.179	5.537	0.062	6.346	0.210	45.77	1.51	129.76
7	603.659	2.648	43.366	0.211	0.0095050	0.0094	12.975	0.114	1.203	0.008	6.388	0.102	46.07	0.75	129.85
8	2343.211	6.501	168.348	0.540	0.0000010	0.0094	36.213	0.171	4.746	0.043	6.149	0.100	44.36	0.74	129.87
9	1482.264	4.540	143.219	0.393	0.0077470	0.0071	21.077	0.059	2.261	0.017	6.055	0.059	43.70	0.46	129.89
10	3030.587	6.597	321.735	1.520	0.0000010	0.0054	33.432	0.062	3.847	0.015	6.171	0.046	44.52	0.38	129.92
11	4648.137	3.449	523.792	0.689	0.0000010	0.0117	44.500	0.148	5.154	0.037	6.209	0.033	44.80	0.30	129.96
12	3924.866	4.590	410.088	0.364	0.0000010	0.0104	38.320	0.145	5.071	0.044	6.191	0.043	44.67	0.36	129.98
13	6025.583	2.051	565.058	0.299	0.0000010	0.0149	95.344	0.153	9.304	0.058	6.203	0.044	44.75	0.37	130.00
Fusion	2957.472	0.792	206.176	0.109	0.0000010	0.0108	147.213	0.304	6.508	0.021	6.249	0.061	45.08	0.47	130.04
K-2															
1	10460.122	12.052	83.333	0.304	0.0092800	0.0127	3.946	0.018	34.496	0.062	6.734	0.690	48.71	4.93	130.67
2	3350.155	27.254	79.059	0.183	0.0000010	0.0116	2.972	0.010	10.187	0.053	5.458	0.448	39.59	3.22	130.68
3	5369.345	10.428	277.963	0.538	0.0000010	0.0136	10.047	0.036	13.046	0.047	5.932	0.101	42.99	0.75	130.70
4	10039.744	8.584	676.698	1.278	0.0000010	0.0086	16.395	0.015	20.740	0.078	6.116	0.066	44.30	0.51	130.74
5	5164.137	2.877	521.205	0.287	0.0000010	0.0114	12.007	0.066	7.102	0.059	6.076	0.044	44.01	0.36	130.76
6	3546.499	1.944	446.407	0.199	0.0000010	0.0081	11.036	0.035	2.977	0.043	6.113	0.034	44.28	0.30	130.78
7	6607.987	6.834	636.049	0.539	0.0000010	0.0054	18.708	0.072	9.778	0.024	6.063	0.035	43.92	0.31	130.80
8	4472.112	2.230	451.542	0.277	0.0000010	0.0094	18.735	0.055	6.206	0.020	6.062	0.032	43.91	0.29	130.84
9	2622.349	7.775	362.682	0.619	0.0000010	0.0111	16.240	0.089	1.653	0.031	6.030	0.037	43.69	0.32	130.87
10	2473.340	10.229	322.387	0.396	0.0018670	0.0100	15.000	0.080	1.950	0.014	6.047	0.039	43.80	0.33	130.89
11	6613.922	2.012	813.253	0.307	0.0000010	0.0104	39.010	0.074	6.105	0.109	6.091	0.044	44.12	0.36	130.91
12	5779.997	2.362	856.311	0.590	0.0000010	0.0109	50.769	0.135	2.361	0.092	6.087	0.034	44.09	0.30	130.95
13	2848.018	0.911	402.828	0.312	0.0000010	0.0091	69.587	0.169	1.801	0.025	6.063	0.023	43.92	0.25	130.97
Fusion	1906.303	0.971	220.643	0.181	0.0000010	0.0089	278.297	0.393	3.272	0.026	6.083	0.043	44.06	0.36	130.99
K-22															
1	6403.636	11.672	124.412	0.135	0.0014840	0.0146	1.537	0.023	20.404	0.101	4.416	0.360	32.16	2.60	133.67
2	3600.474	4.133	304.375	0.426	0.0000010	0.0168	2.200	0.059	6.723	0.074	5.541	0.083	40.26	0.62	133.68
3	10727.783	14.037	1351.797	1.633	0.0000010	0.0130	6.311	0.030	8.944	0.052	6.093	0.025	44.22	0.26	133.70

4	8349.706	5.804	1226.863	0.936	0.0000010	0.0120	4.757	0.054	2.912	0.028	6.182	0.015	44.86	0.21	133.73
5	5358.799	2.870	823.127	0.609	0.0000010	0.0092	3.214	0.033	1.178	0.021	6.157	0.014	44.68	0.21	133.77
6	2696.424	16.509	426.616	1.890	0.0000010	0.0118	1.681	0.033	0.465	0.012	6.064	0.049	44.01	0.40	133.79
7	4075.756	8.328	642.395	1.553	0.0000010	0.0119	2.969	0.019	0.877	0.013	6.010	0.023	43.62	0.24	133.82
8	1989.140	7.010	314.668	1.043	0.0000010	0.0121	1.557	0.023	0.413	0.018	6.002	0.035	43.57	0.31	133.86
9	1848.695	3.812	289.605	0.833	0.0000010	0.0151	1.684	0.033	0.458	0.012	5.988	0.027	43.47	0.26	133.88
10	1844.046	12.395	281.148	0.872	0.0000010	0.0148	2.109	0.040	0.657	0.014	5.948	0.051	43.18	0.41	133.90
11	2753.741	1.347	398.477	0.223	0.0000010	0.0141	4.940	0.031	1.382	0.024	5.982	0.023	43.43	0.24	133.95
12	5518.200	3.830	736.469	0.564	0.0000010	0.0105	7.535	0.043	4.012	0.016	5.993	0.019	43.50	0.22	133.98
13	6717.569	2.406	849.114	0.338	0.0000010	0.0095	13.005	0.065	5.846	0.029	6.005	0.021	43.59	0.24	134.00
14	5411.710	2.309	694.503	0.277	0.0000010	0.0097	9.466	0.022	4.358	0.023	6.060	0.020	43.98	0.23	134.02
Fusion	1537.283	0.676	172.713	0.173	0.0000010	0.0136	2.233	0.015	1.770	0.025	6.025	0.049	43.74	0.39	134.04

$^{40}Ar_{atm}$: atmospheric ^{40}Ar, $^{40}Ar^{*}$: radiogenic ^{40}Ar, Ca: produced by Ca-neutron interferences, K: produced by K-neutron interferences, Age (Ma): the date is calculated using the decay constants recommended by Steiger and Jäger (1977). The errors are at the 1σ level and do not include the error in the value of the J parameter.

Table S2 ($^{143}Nd/^{144}Nd)_{(i)}$ and ($^{87}Sr/^{86}Sr)_{(i)}$ compositions assumed for the end-member components in the assimilation-fractional crystallizations calculation

End member	IC_0 (Parental magma)	IC_A (Upper continental crust)	Total Partition coefficient (∑D)			
				D1	D2	D3
Sr (ppm)	188	350	Sr	1.20	0.50	1.20
Nd (ppm)	9.62	26	Nd	1.85	1.80	1.85
$^{87}Sr/^{86}Sr$	0.7029	0.71463	For all continental crust modelling			
$^{143}Nd/^{144}Nd$	0.51319	0.511843				
	Klein (2004)	Taylor and McLennan (1985)				